LOW-LYING STATES IN ^{95}Tc STUDIED WITH THE ^{93}Nb(α,2nγ)^{95}Tc REACTION

by TOKUSHI SHIBATA

Contents

Synopsis: Low-lying states in ^{95}Tc were studied with the ^{93}Nb(α,2nγ)^{95}Tc reaction. The measurements of the singles γ-ray spectrum, excitation functions of γ-rays, delayed γ-ray spectra, angular distributions of γ-rays and γ-γ coincidence spectra were carried out by use of Ge(Li) detectors.

The following new levels were found on the basis of the results of the γ-γ coincidence measurements; 882 keV, 1516keV, 1550keV,2184keV and 2548keV levels. Spin and parity assignments for several levels are based on the results of the excitation functions of γ-rays and the angular distributions. They are 882 keV $13/2^+$, 957 keV $11/2^+$, 1215 keV $9/2^-$, 1516 keV $17/2^+(13/2)^+$, and 1550 keV $15/2^+(11/2)^+$.

The 336 keV $7/2^+$, 627 keV $5/2^+$, 882 keV $13/2^+$, 957 keV $11/2^+$ states and possibly 1265 keV $9/2^+$ state are found to be strong candidates of the members of the core-multiplet which is generated by the coupling of the $1g_{9/2}$ proton to the E2 phonon of the core. These states are discussed in term of a weak coupling model.

The observed angular distributions of γ-rays were compared with the expectations based on a simple deexcitation model of the (α,2nγ) reaction. The multipolarities of the 336 keV and 957 keV transitions were estimated to be M1+E2(0.6 $\sim$ 12%) and M1+E2(78 $\sim$ 92%), respectively, by referring to the calculated angular distribution.

1. Introduction

The ground state of ^{95}Tc is a $1g_{9/2}$ single quasiproton state.[1-3] This is the only positive parity single quasiparticle state in the major shell between Z=20 and 50, and the spin is the highest. The low-lying states in neighboring doubly even nuclei ^{94}Mo and ^{96}Ru have vibrational character.[4-5] Thus we can expect, in the low excitation energy region of ^{95}Tc, core multiplet states with spins $13/2^+$, $11/2^+$, $9/2^+$, $7/2^+$ and $5/2^+$ by the coupling of this $1g_{9/2}$ proton to the one quadrupole (E2) phonon state of the core. There are no other possibilities for exciting the high-spin states such as $13/2^+$ and $11/2^+$ in the low-excitation region. Therefore these high spin states are likely to be quite pure. One may also expect in the higher excitation region the high-spin states caused by the coupling of $1g_{9/2}$ proton to two and three E2 phonon states of the core. There are a few evidence for the core multiplet states generated by the coupling of the E2-phonon and particles in the high spin state. Low-lying $13/2^+$ and $11/2^+$ states have recently been found in ^{91}Nb[47-48], ^{93}Nb[31-32], ^{93}Tc[48] and ^{115}In[49]. The ground state of these nuclei are all a $1g_{9/2}$ proton state, and the even core of ^{91}Nb, ^{93}Tc and ^{115}In are not of vibrational character. Thus the only nice evidence of core-multiplet has been found in ^{93}Nb.[31-32] Recently Marumori et al.[6-7] have pointed out that the three quasi particle correlation is important for the collective excitation in odd mass nuclei. They have shown that the correlation is quite important for the low spin states in a core-multiplet of spherical odd mass nuclei.[6-7] The purpose of the present work is to study these

core multiplet states (particularly the high-spin states).

Recently Ejiri et al.[8] have shown that the angular distributions of γ-rays following the (α,xn) reaction can be explained using a simple deexcitation model. The model includes the effect of the statistical emission of neutrons, and the statistical and the stretched emissions of γ-rays from the compound nuclei. An expression for the attenuation coefficients for the (α,xn) reaction on the doubly even nucleus has been given.[8] We can expect that the same simple model is also useful for the (α,xn) reaction on the odd nucleus which has finite spin value. It is also the purpose to compare the observed angular distributions with the expectations based on the simple deexcitation model of the (α,xn) reaction.

Previously the level structure of ^{95}Tc has been studied from the radioactive decay of ^{95}Ru,[9-10] and from (p,n),[11-12] (d,n),[1-2] (^{3}He,d),[3] (p,γ)[13] and very recently (p,nγ)[14] reactions. Some low spin levels were studied by these reactions. There is no information so far about high spin states such as 13/2 and 11/2.[15] In the present work we used the ^{93}Nb(α,2nγ)^{95}Tc reaction, since the (α,xnγ) reaction preferentially populates high-spin states. The core multiplet states were well studied by investigating the γ-rays following the (α,2n) reaction. Experimental procedures and results are given in the next section. Detailed discussions on the structure of the core multiplet states are presented in the last section. A part of this work has been published in ref. 45 and 46.

2. Experimental procedures and results

2-1 EQUIPMENTS

Alpha particles with energies 20.5 ∿ 24.5 MeV were provided by the 110 cm Osaka University Cyclotron. The α-particles with energy below 20.5 MeV were obtained by use of aluminium absorbers. The α-beam was guided to a γ-ray cave in a experimental room so as to reduce the back ground γ-rays from a Faraday cup, slit-systems and absorbers. The arangement of the the equipments is shown in fig.1. The target was a metallic Nb-foil with 4 mg/cm^2 in thickness. The Nb-foil was prepared by rolling out a piece of natural Nb-metal. Gamma-rays were detected by 30 cc and 40 cc Ge(Li) crystals (ORTEC) and the 20 cc Ge(Li) detector which was fabricated in our laboratory. The energy resolutions of these detectors were 2.5 keV (30 cc), 3.6 keV (40 cc) and 5.5 keV (20 cc) for the 1.33 MeV γ-ray, respectively. Signals from the Ge(Li) detector were analyzed by a 4096 P.H.A. (PACKARD). Two types of target chamber were used to get the γ-ray spectra. These are shown in fig.2.

2-2 SINGLES γ-RAY SPECTRUM

The singles γ-ray spectrum following the ^{95}Nb(α,2nγ)^{95}Tc reaction with 22.5 MeV α-particles was obtained at 55° with respect to the beam direction by use of the 30 cm^3 Ge(Li) crystal. The obtained singles γ-ray spectrum is shown in fig.3. The energies and the relative intensities of the

γ-rays following the $^{93}Nb(\alpha,2n)^{95}Tc$ reaction are listed in Table 1. The strong 766 keV γ-ray from the β-decay of the ground state of ^{95}Tc appears in the singles γ-ray spectrum, because the spectrum was obtained after a long time irradiation. The energy calibration for the Ge(Li) detector was carried out just before and after the measurement of the singles γ-ray spectrum. The γ-rays from the radio-active decay of ^{133}Ba, ^{137}Cs, ^{60}Co, ^{88}Y and ^{228}Th were used. We obtained the deviations of energies from the values expected from the linear function of channel number by measuring these γ-rays. The correction curve for the energy determination for the Ge(Li) detector is shown in fig.4. Since the spectrum for the energy calibration was obtained after the irradiation in the same geometrical arrangement as for the measurement of the singles γ-ray spectrum following the $(\alpha,2n)$ reaction, the 766 keV γ-ray appeared in both spectra. The peak positions of the 766 keV γ-ray in each spectrum agreed with each other within 0.05 keV. The relative efficiency of the 30 cm^3 Ge(Li) detector was measured for the γ-rays from the β-decay of ^{133}Ba and ^{152}Eu. The relative efficiency curve obtained is shown in fig.5.

We found that some strong transitions feed the ground state ($9/2^+$) and not the isomeric state ($1/2^-$) at 39 keV as follows (see fig.18). We can estimate the intensity of γ-rays feeding the isomeric state at 39 keV. Since the singles γ-ray spectrum was accumulated for the last 4-hours in the total 44 hours irradiation with constant beam current, the total

numbers of the ground state decay in the interval was given by

$$N_\beta(gr) = \int_{t_1}^{t_2} C\,(1 - e^{-\lambda t})\,dt\,, \qquad (2.1)$$

where C is the number of ground state produced by the incident beam per unit time, λ is the decay constant of the ground state ($\tau_{1/2}$=20 hr), t_1=40 hours and t_2=44 hours. From eq.(2.1), we get $N_\beta(gr)/\Delta t \cdot C$=0.77, where Δt=4 hours. The branching ratio for the 766 keV transition to the total β-decay from the ground state is 93.4 %.[15] Thus the number of the ground states produced in the last 4 hours is evaluated as (total number of the 766 keV γ-rays emitted in the interval)/0.77 /0.934. Here we neglected the effect of the conversion electron (<1 %). The isomeric ratio of the ^{93}Nb(α,2n)^{95}Tc reaction has been obtained as $\sigma(9/2^+)/\sigma(1/2^-)$ = 7.0 ± 0.5.[16-17] Thus we get the upper limit of the relative intensity for the γ-rays feeding the isomeric state to be less than 33 (see table 1) by use of the relative intensity of the 766 keV transition. Here we neglected the ^{93}Nb(α,pnγ)^{95}Mo reaction as follows. The 948 keV γ-ray ($9/2^+ \rightarrow 7/2^+$) is expected to be more intense than 766 keV γ-ray ($7/2^+ \rightarrow 5/2^+$) in the ^{93}Nb(α,pnγ)^{95}Mo reaction, because the spin of the emitting state for the 948 keV γ-ray is higher. Indeed the intensity of the 948 keV γ-rays is twice as large as that of the 766 keV γ-ray in the (α,3nγ) reaction.[4] Therefore we can estimate the contribution of the ^{93}Nb(α,pnγ)^{95}Mo reaction to be less than 4 % from the measured intensity of the weak 948 keV γ-ray in the present spectrum. In this way the upper limit of the relative intensity of the γ-rays feeding the isomeric state is estimated to be less

than 33±3. Thus we found that the 882 keV, 633 keV and 957 keV transitions feed the $9/2^+$ ground state, and not the $1/2^-$ isomeric state.

2-3 EXCITATION FUNCTIONS

Excitation functions for γ-rays were measured in an energy range between 17 MeV and 24.5 MeV. We used aluminium absorbers to degrade the α-particle energy below 20 MeV. The excitation functions for γ-rays were used to assign the γ-rays to the appropriate reactions and to estimate the spin values and excitation energies of the emitting states. The observed excitation functions for strong γ-rays are shown in fig.6 and fig.7. Since we are concerned with the relative yields of the γ-rays as a function of the α-particle energy, the erros in the figs. do not include those due to the detection efficiency of the Ge(Li) crystal and the beam collection efficiency. Note that the latter get down a few per-cent as the beam energy decreases because of the spreading by the target and absorbers. These errors amount at most to about 8 %.

2-4 GAMMA-GAMMA COINCIDENCE MESUREMENTS

Gamma-gamma coincidence measurements were carried out at E_α=22.5 MeV. The 40 cm^3 detector was placed at 90° and the 30 cm^3 detector was placed at 70° to the beam direction. The distances between the target and these detectors were 4.5 cm and 5.0 cm, respectively. The beam current was 1.2 nA.

The block diagram of the circuit system is shown in fig.8. The time resolution of the fast coincidence system was set to 40 ns (note that the cyclotron gives 2ns beam bursts every 95 ns). The ratio of chance to true coincidence was less than 3 %. Energy gates were set on the full energy peaks of the 337, 363, 593, 629, 633, 664, 668, 882 and 957 keV γ-rays and the neighboring back ground portions of these photopeaks. Four coincidence spectra were obtained in one run. Each spectra were accumulated for 8 hours. The observed coincidence spectra are shown in fig.9, 10 and 11. The intensities of the coincident γ-rays were obtained by taking the difference of counts with energy gates on and off the photopeaks. The relative intensities obtained from the coincidence spectra and the relative coincidence rate for each gate are given in Table 2.

2-5 DELAYED γ-RAY MEASUREMENTS

The delayed γ-rays were measured with 22.5 MeV α-particles. The block diagrams of the circuit systems for the delayed γ-ray measurement are shown in fig.12. The delay time of the γ-ray was measured by operating a time-to-amplitude converter with starting pulses from Ge(Li) detector and stopping pulses generated by a circuit to pick up the RF signal of the cyclotron oscillater. The circuit diagram to pick up the RF signal is shown in fig.13. Filters tuned to the R-F frequency of the cyclotron oscillater and its higher

harmonics were used to remove the RF modulation on the pulses of Ge(Li) detector. The time modulation was checked by observing the time distribution of γ-rays from radio-active decay. It should be mentioned that we could remove the R-F modulation effectively by wrapping the Ge(Li) detector and the cable between the Ge(Li) crystal and other circuits (main amplifier, H.V.Supply and power supply) by thin aluminium foils (cooking foil).

The delayed γ-ray spectrum was accumulated in a time interval of 15 ns duration starting 20 ns after every beam burst. The lines of the 882, 957, 633 and 593 keV transitions, which were strong in the total γ-spectrum, were not seen in the delayed spectrum. Thus the upper limits of the half lives were estimated to be 3 ns for the 882 and 957 keV transitions, and 5 ns for the 633 and 593 keV transitions.

2-6 ANGULAR DISTRIBUTIONS OF γ-RAYS

The spins of the compound nuclei produced by α-particle in spinless target nuclei are completely aligned in a plane perpendicular to the beam axis. Ejiri et al. have shown that spins of excited states produced in the (α,xnγ) reaction are still aligned in the plane.[8] The degree of the spin alignment of the excited states in low-energy region is well explained by a simple deexcitation model for the target with spin zero.[8] If the target has a finite spin value, which is randomly oriented, the spin alignment of the compound nuclei is not

complete. The spin alignment for high-spin states however is still quite good, if the angular momentum of the incident α-particle is much larger than the target spin value. Therefore the precise measurement of the angular distributions of γ-rays are crucial for the spin assignment of the excited state.

The angular distributions of γ-ray were measured at E_α=22.5 MeV. The angular distributions of γ-ray were measured in 10° steps between 0° and 90°, and at 110°. Here the beam was stopped in a small target chamber, the wall of which was covered with a thin lead sheet (see fig.2b). At foward angle the background from the lead sheet was about 40 % of the total background. Since the energies of some γ-rays from the ^{93}Nb(α,2nγ)^{95}Tc are very close to those from the lead sheet, the measurement was also carried out by using another target chamber, where the beam was guided to a shielded Faraday cup outside the γ-ray cave (see fig. 2a). In this case the γ-rays were measured at 31°, 55°, 70° and 90° to the beam direction. The 20 cm^3 Ge(Li) detector was used as a monitor counter. The distance between the target and the detector is 20 cm and the beam spot was 1.5 mm in width and 4 mm in height. Because of the large distance between the target and the detector, the finite solid angle correction of the detector is small. The corrections are less than 2 % for the A_2 values and less than 4 % for A_4 values.[18] The position of the beam spot was checked every other run at the beam viewer. The position of the beam spot was

satisfactorily constant. The dead time correction in the PHA was made by counting the number of pulses fed to the PHA. The correction was about 1 %. The geometrical asymmetry was checked by measuring the 766 keV γ-ray following the β-decay of ^{95}Tc, which was produced in the target during the measurement of the angular distributions. The results are shown in fig.14 and fig.15. The obtained angular distribution coefficients are given in Table 1.

The angular distribution of γ-rays can be expressed as

$$W(\theta) = 1 + A_2^{max}\alpha_2 P_2(\cos\theta) + A_4^{max}\alpha_4 P_4(\cos\theta) + \cdots \quad (2.2)$$

Here A_2^{max} and A_4^{max} are coefficients for the angular distribution of γ-ray emitted from the completely aligned nucleus,[19] and α_2 and α_4 are attenuation coefficients.

Recently Ejiri et al. have shown that the attenuation coefficients for γ-rays from yrast levels produced by the (α,xn) reaction can be explained by a simple γ-ray deexcitation model. In this model the compound states are considered to decay to the ground state through the following processes. The compound nucleus produced by capture of α-particle decays firstly by the statistical emission of neutrons. Then nucleus reaches to the yrast levels by the successive emissions of statistical γ-rays. Finally nucleus comes to the ground state after emitting the stretched γ-ray through the yrast line. Thus the yrast levels are considered to be fed partially

by the stretched transition from the upper yrast level and partially by the statistical γ-rays from outside the yrast level, which is called as "side feeding". Intensities of the side feeding to each yrast levels are assumed to be constant (see ref.8 and ref.4). The attenuation coefficient $\alpha_2(J_i)$ for levels in even nuclei with spin J_i is given as follows (see ref.8)

$$\alpha_2(J_i) = \frac{1}{J_m+1-J_i} \sum_{J'=J_i}^{J_m} \left[\left(1-\frac{3}{2}\cdot\frac{\frac{1}{3}j_n^2+j_n}{(J'+\frac{1}{2})^2}\right)^{N_n}\cdot\left(1-\frac{3}{2}\cdot\frac{\frac{1}{3}j_\gamma^2+j_\gamma}{(J'+\frac{1}{2})^2}\right)^{N_\gamma}\right.$$

$$\left.\times\left(1-\frac{3}{2}\cdot\frac{1}{J_i+\frac{1}{2}}+\frac{3}{2}\cdot\frac{1}{J'+\frac{1}{2}}\right)\right] \qquad (2.3)$$

Here J_m is the maximum spin of the observed yrast level, N_n and N_γ are the average numbers of neutrons and γ-rays which are emitted during the deexcitation to the yrast level, and j_n and j_γ are mean values of angular momenta carried away by neutrons and γ-rays. The values of j_n and j_γ are obtained from the conventional statistical model. Eq. (2.3) is derived for the case in which the spins of incident particle and target nucleus are both zero, and thus the spins of the compound nuclei are completely aligned. Assuming that the deexcitation process in odd A nuclei is essentially the same as in even nuclei, we apply eq. (2.3) for the present case.

Here the target spin is $9/2^+$, which is randomly oriented. The correction for target spin J_t is given as

$$B_2(J_c)=\left[\sum_{\ell=|J_c-J_t|}^{J_c+J_t}\frac{2J_c+1}{2J_t+1}T_\ell U_2(\ell\xrightarrow{J_t}J_c)\right]\Big/\left[\sum_{\ell=|J_c-J_t|}^{J_c+J_t}\frac{2J_c+1}{2J_t+1}T_\ell\right] \tag{2.4}$$

Here J_c is spin of the compound state, ℓ is the angular momentum introduced into the target by the α-particle, and T_ℓ is the transmission coefficients for the α-particle (numerical values are available in ref.20). The factor U_2[21] is given by

$$U_2(\ell\xrightarrow{J_t}J_c)=(2\ell+1)^{1/2}(2J_c+1)^{1/2}W(\ell\ 2\ J_t\ J_c;\ \ell\ J_c). \tag{2.5}$$

The values $B_2(J_c)$ are shown for the present case in fig.16. We obtain the attenuation coefficent for the state with spin J_i as follows

$$\alpha_2(J_i)=\frac{1}{J_m+1-J_i}\sum_{J'=J_i}^{J_m}B_2(J')\left[\left(1-\frac{3}{2}\cdot\frac{\frac{1}{3}j_n^{\,2}+j_n}{(J'+\frac{1}{2})^2}\right)^{N_n}\left(1-\frac{3}{2}\cdot\frac{\frac{1}{3}j_\gamma^{\,2}+j_\gamma}{(J'+\frac{1}{2})^2}\right)^{N_\gamma}\right.$$
$$\left.\times\left(1-\frac{3}{2}\cdot\frac{1}{J_i+\frac{1}{2}}+\frac{3}{2}\cdot\frac{1}{J'+\frac{1}{2}}\right)\right] \tag{2.6}$$

We use the values $N_\gamma=3$, $N_n=2$, $j_n=1.2$ and $j_\gamma=1.2$ from the

conventional statistical model (see Appendix 1). The maximum spin value of the states populated in the present reaction is taken as J_m=21/2 (see sec.2-7), and this agrees with the maximum angular momentum introduced into the compound nucleus by the α-particle bombardment. (A change of one unit in J_m causes a change of about 0.025 in α_2.)

Angular distributions of γ-rays following the (α,2n) reaction on deformed nuclei with high-spin have been measured.[22-26] The attenuation coefficients obtained from the angular distributions for the targets with spin 5/2 and 7/2 are shown in fig.17 together with the present results. We note that the attenuation coefficients depend little on the incident energy and Q-value, and that they only depend on the spin value of the excited state. There are a few data of attenuation coefficients for the (α,2n) reaction on odd mass targets and the obtained values have large errors, therefore we couldn't derive the definite conclusion about the validity of eq. (2.6). It is interesting to investigate the angular distribution with odd mass target in order to make clear the mechanism of the reaction and to use the (α,xn) reaction as an efficient spectroscopic tool. The agreement of the calculations and obtained values are satisfactory, and the deviation from calculated values are smaller than 0.1 for α_2.

2-7 LEVEL SCHEME

We propose a level scheme for ^{95}Tc as shown in fig.18

on the basis of following results and arguments. The ground state $9/2^+$ and the isomeric state $1/2^-$ at 39 keV have been well established.[15)]

The 336.6 keV level. The spin and parity assignment of $7/2^+$ has been established by previous works.[9-11,27)] An M1+E2 (11 ± 9 %) multipole for the 337 keV transition has been reported from conversion electron measurement.[27)] The mixing ratio is obtained from the present results of the γ-ray angular distribution. Using an attenuation coefficient $\alpha_2 = 0.29 \pm 0.1$ for the $7/2^+$ state, which was estimated from fig.17, the quadrupole dipole amplitude mixing for the 337 keV transition is obtained as $\delta = 0.08 \sim 0.36$, where $\delta = \langle f||E2||i\rangle/\langle f||M1||i\rangle$. This is graphically shown in fig.19. Thus the 337 keV transition is mostly of M1 character with small E2 admixture (0.6 % ∿ 12 %). This is consisten with results from conversion electrom measurements.[27)] It should be mentioned that the other possibility of $\delta = 4 \sim \infty$ is not excluded from present results because of a large error in the A_4 coefficient (see fig.19).

The 626.9 keV level. A level around 627 keV is known from the ^{95}Ru decay,[9-10)] the (d,n) reaction,[1)] (p,n) reaction,[11)] and (p,γ) reaction studies.[13)] The spin and parity of this state has been assigned as $5/2^+$[1,9,10,13)] The excitation function for the 626.9 keV γ-ray observed in the present work shows that the spin of the emitting state of the γ-ray shoud be around 5/2. Thus the present 626.9 keV γ-ray is

considered to be the ground state transition from the $5/2^+$, 627 keV state.

The 646.8 keV level. This level has been observed in the (p,n) reaction[11-12], the ^{95}Ru decay[10], the (p,γ) reaction[13] and the particle transfer reaction.[2.3] The spin and parity of this state has been established to be $3/2^-$ by the (p,n) reaction[12]. The excitation function for the present 607.9 keV γ-ray suggests a low spin for the emitting state. Thus this γ-ray fits in the transition from the 646.8 keV state to the 38.9 keV first excited state.

The 667.9 keV level. The 667 keV state has been observed in the (p,n) reaction[11] and the (p,γ) reaction.[13] The 629.0 keV γ-ray was assigned to the transition from this level to the38.9 keV state. The energy sum of a cascade transition of the 38.9 - 629.0 - 546.8 keV agrees well with the 1214.7 keV cross over transition. The spin of this state has been established to be $5/2^-$ by the (p,n) reaction[12]. The excitation function for the 629.0 keV γ-ray is consistent with the $5/2^-$ assignment.

The 882.4 keV level. We propose this level on the basis of the following reasons. 1) The 882.4 keV γ-ray is the strongest and no other γ-rays with a compatible intensity is seen both in the singles spectrum and in the coincidence spectra above 50 keV. 2) This γ-ray feeds the ground state, and not the isomeric state (see sec. 2-2). 3) The energy sums of the two cascade lines of the 882.4 keV - 667.2 keV

and the 957.3 keV - 592.5 keV agree well with each other. This locates the excited states at 882.4 keV and 1549.7 keV (the 957.3 keV state has been observed in the (p,n) reaction.) The spin of this state is assigned as 13/2 on the basis of the following facts. a) The results of delayed γ-ray spectrum show that the multipolarity of the 882.4 keV transition is smaller than 3. Therefore the possible spin value is restricted to the values between 5/2 and 13/2. b) The fact that the sign of the angular distribution coefficient A_4 is negative indicates that the spin of this state is either 9/2 or 13/2. (see fig.19) c) The excitation function for the 882.4 keV γ-ray rises more rapidly than that for the 957 keV with spin 11/2. This shows that the spin of this state is not smaller than 11/2. (see below) The spin assignment 13/2 for the 882 keV state is consistent with the following facts. 1) The branching to the 337 keV $7/2^+$ state is known to be less than 2 % from the present results of the γ-γ coincidence measurement. 2) This state has not seen from the ^{95}Ru decay. 3) The (p,n) reaction little populate this level [11], suggesting that the spin of this state is high. The positive parity assignment for the 882 keV state is based on the following. If it were of negative parity, the 882 keV transition to the $9/2^+$ ground state would be of M2 character. Recently Ejiri et al. have shown that the spin-isospin core polarization reduces very much M2 transition rates between single-quasiparticle states.[28] If we take the same reduction rate as in ref.28, the expected

half-life for the single-particle 882 keV transition would be longer than 5 ns. However the delayed spectrum indicates no delayed component for the 882 keV.

The 928.1 keV level. The spin and parity assignment of $(5/2^+)$ has been reported from the ^{95}Ru decay studies.[9-10] The present results of the γ-γ coincidence measurements show the 301.2 - 290.6 - 336.6 keV cascade transitions as seen in the ^{95}Ru decay. Since the 301.2 keV transition is very weak, we can not get further information about this level.

The 957.3 keV level. The location of this level is based on the following reasons. 1) There is no intense γ-ray in coincidence with this γ-ray above 50 keV. 2) This γ-ray feeds the ground state and does not feed the isomeric state at 38.9 keV. 3) An excited state at 960 keV has been observed in the (p,n) reaction.[11] The spin is assigned to be 11/2 on the following bases. a) The results of the delayed γ-ray measurement indicate the multipolarity of this transition to be L=1 or 2. b) The sign of the A_4 coefficient of the γ-ray angular distribution is positive. Thus the spin of this state is 7/2 or 11/2. c) The value of $A_4/A_0=0.067\pm0.018$ would give the atenuation coefficient 38 ± 10 % for the A_4 coefficient, if the spin were 7/2. Then using a Gaussian distribution of the substate population,[19] the attenuation coefficient α_2 would get as large as 65 ∿ 85 %, which is too large by referring to both the empirical and calculated values (see sec.2-6 and fig.17). d) The excitation function for the 957.3 keV γ-rays

rises more rapidly than that for the 336.6 keV. This suggests the spin of this state to be higher than 7/2. The parity of this state is probably positive, because the observed angular distribution shows mixed multipolarities for the 957.3 keV transition. Thus M1+E2 is most likely. The $11/2^+$ assignment is consistent with the results of the β-decay of ^{95}Ru. This state is not populated by the ^{95}Ru decay, thus the log ft value of the β-transition to this state is larger than ∿7[10]. This may exclude a $7/2^+$ assignment.

The mixing ratio of M1 and E2 amplitude is estimated using an attenuation coefficient $\alpha_2 = 0.45 \pm 0.1$ (see fig.17). The attenuation coefficient for the term A_4P_4 was estimated to be $\alpha_4 = 0.13 \pm 0.07$ using a Gaussian distribution for the substates[19]. The mixing ratio obtained is $\delta = -2.6\ ^{+0.7}_{-0.9}$ which is graphically shown in fig.19. Recently the low-lying states in ^{95}Tc were studied by the (p,nγ) reaction[14]. The 882 keV and 957 keV states were observed in the (p,nγ) reaction. The spin and parity assignments are consistent with our present results.

The 1085.4 keV level. An excited state at about 1085 keV has been reported in the ^{95}Ru decay[10] and in the (p,n) reaction studies[11]. An excited state with spin $(5/2^+)$ at around 1085 keV has also been reported from the particle transfer reaction studies[2-3]. The results of the γ-γ coincidence measurements indicate that the 748.8 keV γ-ray is the transition from the 1085.4 keV state to the 336.6 keV state.

The 1179.0 keV level. This level is known from ^{95}Ru decay[9-10] and the (p,n) reaction[11]. The 1179 keV γ-ray in the present work seems to be the transition from the 1179 keV state to the ground state.

The 1214.7 keV level. The location of this level has been reported by the (p,n) reaction studies[11]. The results of γ-γ coincidence measurements indicate that the transition from this state feed the 667.9 keV 5/2 , 336.6 keV $7/2^+$ and ground $9/2^+$ states. These γ-branches restrict the spin of this state to $5/2^+$, $7/2^+$, and $9/2^-$. This state is not populated in the ^{95}Ru decay, suggesting the spin of this state to be $7/2^-$ or $9/2^-$. The signs of the A_2 coefficients of the angular distribution of the 547, 879 and 1215 keV γ-rays show the spin of this state to be $9/2^-$. Here we assumed that the E1 transitions are pure.

The 1515.5 keV level. This state is proposed on the basis of the following reasons. 1) The 633.1 keV γ-ray is in coincidence with the 882.4 keV γ-ray. 2) There is no more intense γ-ray than the 633 keV γ-ray which is in coincidence with the 882 keV γ-ray above 50 keV. The spin assignment of $17/2^+$ ($13/2^+$) to this state is based on the following reasons. a) The result of the delayed γ-ray measurement indicates that the multipolarity of the 633 keV transition is smaller than 3. b) The sign of the A_4 coefficient is negative. This fact, together with the obtained value of the A_2/A_0 restricts the spin of this state to 17/2 or 13/2. c) The excitation function

for the 633 keV γ-ray rises more rapidly than that for the 882 keV. d) The upper limits of the branchings to the 957 keV and the ground states are all less than 1 %. The parity of this state is probably positive because of the following reasons. The 15/2 assingnment gives an L=2 multiporaity for the 633 keV transition. An M2 transition is improbable from the upper limit of the half life (see sec.2-5). A 13/2 assignment means the mixed transition of L=1 and 2, referring to the A_2/A_0 coefficient, in this case an M1 and E2 mixing is most probable.

The 1549.7 keV level. As already mentioned, the two casade lines of 592 keV - 957 keV and the 667 keV - 882 keV locate an excited state at 1549.7 keV. The spin and parity assignment of $15/2^+$ ($11/2^+$) is based on the reasons similar to those for the 1515.5 keV state.

The 2184.2 keV and the 2547.5 keV levels. These states are proposed on the basis of the cascade transitions of 363 keV - 669 keV - 633 keV and 1032 keV - 633 keV. The excitation functions for the 363, 669 and 1032 keV γ-rays show that the spins of these states are high. The angular distribution of 1032 keV γ-ray has a shape of a stretched E2 transition type. Thus one may assign 21/2 for the 2547.5 keV state.

The 1264.5 keV level. We can expect the $9/2^+$ state by the coupling of the 1g9/2 proton to the E2 phonon at around 870 keV (the excitation energy of the first 2^+ state in ^{94}Mo). The $9/2^+$ state at 1.24 MeV or 1.27 MeV has been reported by

the (^{3}He,d)[3] and the (d,n)[2] reaction studies, respectively. The present 1264.5 keV γ-ray may be the transition from the $9/2^{+}$ state to the ground state.

1276.4 keV level. The 1273.5 keV γ-rays seem to deexcite from the 1278 keV state which has been reported by the (p,n) reaction[11] and (p,γ) reaction studies.[13]

The 1702.4 keV and the 2213.3 keV levels. These excited states are tentatively located on the basis of the γ-γ coincidence measurements.

3 Discussion

The excited states produced by the coupling of the 1g9/2 single proton to the E2 phonon of the core ^{94}Mo are expected in the low excitation region of ^{95}Tc. The high spin states in the multiplet such as 11/2 and 13/2 are expected to be quite pure on the basis of the following reasons. 1) The ground state of the ^{95}Tc is the 1g9/2 single quasiparticle state[1-3]. This state is the only positive parity state in the major shell between Z=20∿50, and the spin is the highest. 2) The energies of the low-lying states in ^{94}Mo are of vibrational character[4,29] (see fig.20). 3) The results from Coulomb excitation studies on ^{94}Mo[5] indicate that the matrix elements between one and two phonon states are close to the values expected from the vibrational model. The matrix elements between one and two phonon states are given[30] by

$$|\langle \lambda 2 \| Q \| 21 \rangle|^2 = \frac{2(2\lambda + 1)}{5} |\langle 21 \| Q \| 00 \rangle|^2, \qquad (3.1)$$

where the state $|\lambda N\rangle$ indicates the N-phonon state with the spin λ, and Q is the mass quadrupole moment operator. The matrix elements are obtained from the B(E2) values by the relation

$$B(E2, I_i \longrightarrow I_f) = \frac{1}{2I_i + 1} |\langle I_f \| Q \| I_i \rangle|^2. \qquad (3.2)$$

The matrix elements in ^{94}Mo obtained from Coulomb excitation studies agree with the expected values from eq.(3.1) (Table 3).

4) The structure of the neighboring odd nucleus ^{93}Nb was studied by Coulomb excitation.[31-32] The multiplet levels in ^{93}Nb are located in a small energy region and energies are close to the first 2^+ state in the core ^{94}Mo (see fig.20). The measured B(E2) values for the 11/2 and 13/2 states are close to the values expected from the weak coupling model, although the B(E2) values for the 5/2 and 7/2 states are larger than the expected values (see the follows). In the framework of the weak coupling model, the B(E2) values for the transitions from the multiplet states to the ground state are expressed by

$$B(E2,\ I_i \longrightarrow I_f) = \frac{2I_f + 1}{5(2I_i + 1)}\ B(E2,\ 0 \longrightarrow 2)_c \qquad (3.3)$$

where I_i and I_f are spins of the ground state and the multiplet states, and the $B(E2)_c$ is the B(E2) value for the one phonon state in the core. The values obtained from Coulomb excitation and the values given by eq.(3.3) are listed in Table 3.

In the low excitation region of ^{95}Tc, we found the excited states $(5/2^+)$ (627 keV), $7/2^+$ (337 keV), $11/2^+$ (957 keV), $13/2^+$ (882 keV) and possively $9/2^+$ (1265 keV). These states are probably candidates of the multiplet expected from the coupling of the 1g9/2 single proton to the E2 phonon of the core. The energy levels of these multiplet states in ^{95}Tc and ^{93}Nb are shown in fig.20 together with the levels in negiboring even nuclei.

It is interesting to note following facts. 1) The level

sequence of the multiplet in ^{95}Tc is the same as in ^{93}Nb[31]. 2) The core multiplet levels in ^{95}Tc are spread in energy although those in ^{93}Nb are concentrated in a small energy region. 3) The energies of the high-spin levels such as 11/2 and 13/2 states in ^{93}Nb are very close to the energy of the first 2^+ state in neighboring doubly even nucleus ^{92}Zr, and those in ^{95}Tc are very close to the first 2^+ state energy in ^{94}Mo (see fig.20). 4) The energies of $(15/2^+)$ (1550 keV) and $(17/2^+)$ (1516 keV) states are close to the energy of the first 4^+ state in ^{94}Mo.

Now let's compare the present results with various model calculations. The Hamiltonian for the core multiplet is given as follows in terms of a conventional weak coupling model

$$H = H_c + H_p + H_{int} , \tag{3.4}$$

where H_c and H_p are the Hamiltonians for the core and the odd particle, respectively. Now we take only a quadrupole interaction as

$$H_{int} = -\chi Q_c^{(2)} \cdot Q_p^{(2)} \tag{3.5}$$

where $Q_c^{(2)}$ and $Q_p^{(2)}$ are the mass quadrupole moment operators of the core and the particle, respectively, and χ is the strength parameter of the interaction. The matrix element of the Hamiltonian is given by [33]

$$\langle J_c'N'j_p' \; I \; M \,|H|\, J_cNj_p \; I \; M\rangle = \delta_{J_c'J_c} \, \delta_{j_p'j_p} \, \delta_{NN'} \, (N\hbar\omega + E_{j_p})$$

$$+ \varepsilon(J_c'N', J_cN, I) , \tag{3.6}$$

$$\varepsilon(J_c'N', J_cN, I) = -\chi W\,(2j_p\ J_c\ I;\ j_pJ_c')\langle J_c'N' \| Q_c^{(2)} \| J_cN\rangle$$

$$\times \langle j_p \| Q_p^{(2)} \| j_p\rangle. \qquad (3.7)$$

Where J_c is the phonon spin, N is the phonon number, and j_p is the odd particle spin. The I and M are the total spin and its z-component. We take into account zero, one and two phonon states in the even core, and the 1g9/2 state as the odd particle. Here the 1g9/2 is the only single particle state with positive parity state in the major shell, and we are presently concerned only with positive parity states. Then the energies of the ground state and the multiplet are expressed as follows.

$$E^{g.s} = E_{j_p} - \frac{1}{\hbar\omega}\,[|\varepsilon(21,00,I)|^2] - \frac{1}{\hbar\omega}\,[\tfrac{1}{2}|\varepsilon(22,00,I)|^2$$

$$+ \frac{1}{20}\{\varepsilon(42,42,I) + \varepsilon(22,22,I) + 2\varepsilon(21,21,I)\}^2], \qquad (3.8)$$

for the ground state and

$$E^I = \hbar\omega + E_{j_p} - \frac{1}{\hbar\omega}\,[|\varepsilon(42,21,I)|^2 + |\varepsilon(22,21,I)|^2$$

$$+ |\varepsilon(02,21,I)|^2\delta_{I,j_p} - |\varepsilon(21,00,I)|^2\delta_{I,j_p}] + [\varepsilon(21,21,I)$$

$$- \frac{1}{8\hbar\omega}\{\varepsilon(42,42,I) + \varepsilon(22,22,I) - 2\varepsilon(21,21,I)\}^2], \qquad (3.9)$$

for the multiplet. Here we neglected the term $(\varepsilon/\hbar\omega)^2$, since

the observed energy difference between the 11/2 and 13/2 states is much smaller than the phonon energy.

As an extreme case, we firstly take a simple vibrational motion of a spherical even core, where the quadrupole matrix element $\langle J_c' N' \| Q \| J_c N \rangle$ has non vanishing value only when $\Delta N = N' - N = \pm 1$. Then both the last terms in eq.(3.8) and the last term in eq.(3.9) vanish. The values $\hbar\omega$ and $\langle \| Q_c^{(2)} \| \rangle$ for the even core are taken from the phonon energy in ^{94}Mo and Coulomb excitation data (see Table 3). We used the value $|\langle 02 \| Q_c^{(2)} \| 21 \rangle|^2 = 872$ fm^2 expected from the eq.(3.1) since the Coulomb excitation value is not available. The matrix element for the single particle state is given by[34]

$$\langle n_2 \ell_2 j_2 \| f(r) Y_\lambda \| n_1 \ell_1 j_1 \rangle$$

$$= i^{\ell_1 - \ell_2} (-)^{j_1 + \lambda - j_2} \left\{ \frac{(2\lambda+1)(2j_1+1)}{4\pi} \right\}^{1/2} (j_1 \tfrac{1}{2}\ \lambda 0 \,|\, j_2 \tfrac{1}{2}) \langle j_2 | f | j_1 \rangle \tag{3.10}$$

$$\langle j_2 | f | j_1 \rangle = \int R_{n_2 \ell_2 j_2}\ f(r)\ R_{n_1 \ell_1 j_1}\ r^2 dr$$

The values of $\langle j_2 | r^2 | j_1 \rangle$ are evaluated by use of the harmonic oscillator wave functions.[35] We get $\langle g9/2 \| r^2 Y_{20} \| g9/2 \rangle = 24.9$ fm^2 for the potential parameter $\hbar\omega_0 = 41\ A^{-1/3}$ MeV. Using these values, the energies for the multiplet can be given as functions of the strength parameter χ. The results are shown in fig.21. We note there that the level order of the 11/2 and 13/2 states disagree with the observed values, and the $7/2^+$

and $5/2^+$ levels are not as low as observed. Coupling with the g7/2 single particle level in the upper major shell might contribute to the $11/2^+$ level. However it pushes down to opposit direction. Therefore one may conclude that the simple vibrational model fails to reproduce the experiment.

In order to reproduce the level order of the $11/2^+$ and $13/2^+$ levels, which are quite pure, in a framework of the vibrational model we have to introduce the non zero values for diagonal quadrupole moment $\langle J_c' N \| Q_c^{(2)} \| J_c N \rangle \neq 0$. The values of the diagonal elements for the two phonon states were assumed to be given by

$$\langle J_c 2 \| Q_c^{(2)} \| J_c 2 \rangle = 2(-)^{J_c}(2J_c+1)\langle 21 \| Q_c^{(2)} \| 21 \rangle W(2\ J_c\ 2\ J_c;\ 22 \rangle \tag{3.11}$$

The phonon energy and diagonal element of the one phonon state of the core are adjusted so as to reproduce the energies of the 11/2 and 13/2 states for given χ value. The results are shown in fig.22 and fig.23. It is interesting to note that the phonon energy and the diagonal element do not change with the strength χ very much but the energies of multiplet change remarkably. The interaction strength χ is given[36] by

$$\chi \simeq \left(\frac{m\omega_0}{\hbar} \right)^2 \frac{240}{A^{5/3}} \text{ MeV} \tag{3.12}$$

This gives $\chi \simeq 5.5$ keV fm^{-4}. This strength agrees with the value shown by Kisslinger et al.[37] and Matsuyanagi et al.[38]. The single particle matrix element should be replaced by $\langle j \| Q_p^{(2)} \| j \rangle (U_j^2 - V_j^2)$ for the quasiparticle state. We can

use the U.V. factors obtained from particle transfer reaction studies.[1-3,39] We get $U_j^2 - V_j^2 = 0.3 \sim 0.5$. Since we can include the factor $(U^2 - V^2)$ into the strength χ, we take the strength parameter to be $\chi \simeq (U_j^2 - V_j^2) \times 5.5$ keV fm^{-4} = (1.7 $\sim$ 2.7) keV fm^{-4} in fig.22 and fig.23. Thus we get the values $\hbar\omega$ = 950 keV and $\langle 21 \| Q_c^{(2)} \| 21 \rangle = -17$ fm^2 for the strength 2.7 keV fm^{-4}. The energies of the multiplet states are shown in fig.24(A) for these values. A general trend of the level sequence is qualitatively in agreement with the experiment except for the $7/2^+$ levels. In other wards the effect of the interaction which is not included in the pure vibrational model might be represented by the non-zero values for the diagonal Q-matrix element. The same calculations for the ^{93}Nb give the values $\hbar\omega \simeq$ 1 MeV and $\langle 21 \| Q_c^{(2)} \| 21 \rangle \simeq -12$ fm^2 (see fig.25, 26). If the even core ^{92}Zr consists mostly of the $(d5/2)^2$ configuration, the sign of the diagonal element should be the positive.

Recently Marumori et al. have shown that the three quasi-particle correlation is very important in the collective excitation of odd nucleus. The calculation including this correlation was carried out by Matsuyanagi et al. The results are shown by (B) and (C) in fig.24.[38] The result (B) is obtained by adjusting the strength of the Q-Q interaction so as to reproduce the excitation energy of the $7/2^+$ state. The result (C) is obtained by including the 1g7/2 and 2d5/2 odd proton states (the upper major shell) in

addition to the 1g9/2 proton state. The agreement is satisfactory. Interesting is to note that the change of two units in proton number from ^{93}Nb to ^{95}Tc yields the large spreading of the core multiplet, suggesting an importance of the three quasi particle correlation. The systematic investigation of the structure in the low excitation region of the odd mass nuclei in this region is very important to make clear the effect of the coupling of the particle to the core.

Acknowledgement

The author wishes to thank Professor T.Wakatsuki for valuable suggestions and encouragements during the course of this work. The author would like to express his cordial thanks to Professor H.Ejiri for valuable discussions and his critical comments. The valuable discussions with Professors M.Sano, Y.Yoshizawa and T.Marumori are gratefully acknowledged. The author is also grateful to Dr. K.Matsuyanagi for his calculations and valuable discussions and is greatly indebted to Dr. T.Itahashi for his excellent collaboration.

Appendix I Statistical calculations for Evaporated Neutrons and Gamma Rays.

A neutron evaporation probability is proportional to the penetration coefficient of the neutron and the level density of the nucleus after evaporation of the neutron. Thus the probability is written as

$$Y_{\ell_n}(E_n) = (2\ell+1)\, T_{\ell_n}(E_n) \exp(2E/T), \qquad \text{(A1.1)}$$

where $T_{\ell_n}(E_n)$ is the penetration coefficient for the neutron with an energy E_n and an orbital angular momentum ℓ_n. This value can be calculated easily.[43] The values of calculated $T_{\ell_n}(E_n)$ are shown in fig.28 for $\ell_n = 0$, 1, 2 and 3. The nuclear temperature T is given[44] by

$$T = \sqrt{E/a} \cong \sqrt{7.2E/A} \qquad \text{(A1.2)}$$

where A is the mass number. The mean value of the neutron energy E_n is estimated to be 0.8 MeV for the present $^{93}Nb(\alpha,2n)^{95}Tc$ reaction. The mean value of the orbital angular momentum ℓ_n is given by

$$\ell_n(E_n) = \frac{\Sigma \ell (2\ell + 1)\, T_{\ell_n}(E_n)}{\Sigma (2\ell + 1)\, T_{\ell_n}(E_n)} \qquad \text{(A1.3)}$$

The values of $\ell_n(E_n)$ is shown in fig.27. From fig.27, we get $\ell_n \simeq 1$. Thus the mean value j_n is estimated to be $j_n \simeq 1.2$ summing up the spin of the neutron.

A gamma emission probability is obtained by

$$Y(E_j) = kE_j^3 \exp(2E/T). \qquad (A1.4)$$

Here we assumed $j_\gamma \simeq 1$. Using eq.(A1.4), we get $N_\gamma \sim 3$ ($E_\gamma \sim 1.3$ MeV). It is known that statistical gamma rays are mostly of dipole character, but they contain 10 ∿ 20 % of quadrupole transition. Therefore we used $j_\gamma \lesssim 1.2$ for the present analysis.

Reference

1) J.Bommer, H.Fuchs, K.Grabish, H.Kluge and G.Röschert: Nucl. Phys. A173 (1971) 383.

2) R.J.Riley, J.H.Horton, C.L.Hollas, S.A.A.Zaidi, C.M.Jones and J.L.C.Ford, Jr.: Phys. Rev. C4 (1971) 1864.

3) Y.Shamai, D.Ashery, A.I.Yavin, G.Bruge and A.Chaumeaux: Nucl. Phys. A197 (1972) 211.

4) C.M.Lederer, J.M.Jaklevic and J.M.Hollander: Nucl. Phys. A169 (1971) 449.

5) J.Barrette, M.Barrette, A.Boutard, R.Haroutunian, G.Lamoureux and S.Monaro: Phys. Rev. C6 (1972) 1339.

6) A.Kuriyama, T.Marumori and K.Matsuyanagi: Prog. Theor. Phys. 45 (1971) 784.

7) A.Kuriyama, T.Marumori and K.Matsuyanagi: Prog. Theor. Phys. 47 (1972) 498.

8) H.Ejiri, T.Shibata, A.Shimizu and K.Yagi: J. Phys. Soc. Japan 33 (1972) 1515.
H.Ejiri, M.Ishihara, M.Sakai, K.Katori and T.Inamura: Phys. Letters 18 (1965) 314: Nucl. Phys. 89 (1966) 641.

9) A.B.Tucker and W.W.Hein: Nucl. Phys. A155 (1970) 129.

10) A.C.Xenoulis and D.G.Sarantites: Phys. Rev. C7 (1973) 1193.

11) H.J.Kim, R.L.Robinson, C.H.Johnson and S.Raman: Nucl. Phys. A142 (1970) 35.

12) H.J.Kim, R.L.Robinson and C.H.Johnson: Nucl. Phys. A167 (1971) 65 and H.J.Kim, and R.L.Robinson: Nucl. Phys. A167 (1971) 73.

13) D.A.Close and R.C.Bearse: Nucl. Phys. A201 (1973) 337.

14) D.G.Sarantites and A.C.Xenoulis: private communication 1974.

15) L.R.Medsker and D.J.Horen: Nuclear Data Sheets B8 No.1 (1972) 29.

16) T.Matsuo, J.M.Matsuzek, Jr., N.D.Dudey and T.T.Sugihara: Phys. Rev. 139 (1965) B886.

17) P.Bond and S.Jha: Phys. Rev. C2 (1970) 1887.

18) K.S.Krane: Nucl. Instr. 98 (1972) 205,
J.Barrette, G.Lamoureux and S.Monaro: Nucl. Instr. 93 (1971) 1,
D.C.Camp and A.L.Van Lehn: Nucl. Instr. 76 (1969) 192.

19) T.Yamazaki: Nuclear Data A3 No.1 (1967) 1.

20) J.R.Huizenga and G.Igo: Argonne National Laboratory report ANL-6373 (1961).

21) J.O.Rasmussen and T.T.Sugihara: Phys. Rev. 151 (1966) 992.

22) J.O.Newton: Nucl. Phys. A108 (1968) 353.

23) S.A.Hjorth, H.Ryde, K.A.Hagemann, G.Løvhøiden and J.C.Waddington: Nucl. Phys. A144 (1970) 513.

24) G.Winter, L.Funke, K.Hohmuth, K.H.Kaun, P.Kemnitz and H.Sodan: Nucl. Phys. A151 (1970) 337.

25) B.Skanberg, S.A.Hjorth and H.Ryde: Nucl. Phys. A154 (1970) 641.

26) G.Winter, L.Funke, K.H.Kaun, P.Kemnitz and H.Sodan: Nucl. Phys. A176 (1971) 609.

27) M.E.Phelps and D.G.Sarantites: Nucl. Phys. A171 (1971) 44.

28) H.Ejiri, T.Shibata and M.Fujiwara: Phys. Rev. C8 (1973) 1892.

29) M.T.McEllistrem, K.Sinram, C.E.Robertson and J.D. Brandenberger: Bull. Am. Phys. Soc. 16 (1971) 1154.

30) K.W.Ford and C.Levinson: Phys. Rev. 100 (1955) 1.

31) P.H.Stelson, R.L.Robinson, W.T.Milner, F.K.McGowan and M.A.Ludington: Bull. Am. Phys. Soc. 16 (1971) 619.

32) M.Kregar and G.G.Seamann: Nucl. Phys. A179 (1972) 153.

33) V.K.Thankappan and W.W.True: Phys. Rev. 137 (1965) B793.

34) A.Bohr and B.Mottelson: Nuclear Structure, Vol.1 (Benjamin, 1969).

35) S.Yoshida: Phys. Rev. 123 (1961) 2122,
S.Yoshida: Nucl. Phys. 38 (1962) 383.

36) D.R.Bes and R.A.Sorensen, The pairing-plus-quadrupole model, Advances in Nuclear Physics (Plenum Press), Vol.2 (1969) 129.

37) L.S.Kisslinger and R.A.Sorensen: Kgl. Danske Videnskab. Selskab. Mat-Fys. Medd. 32 No.9 (1960)

38) A.Kuriyama, T.Marumori and K.Matsuyanagi: Prog. Theor. Phys. 51 (1974) 779.

39) H.Ohnuma and J.L.Yntema: Phys. Rev. 176 (1968) 1416.

40) D.C.Kocher and D.J.Horen: Nuclear Data Sheets B7 No.4 (1972) 299.

41) L.R.Medsker: Nuclear Data Sheets B8 No.6 (1972) 599.

42) D.C.Kocher: Nuclear Data Sheets B8 No.6 (1972).

43) J.M.Blatt and V.F.Weisskoph: Theoretical Nuclear Physics (John Wiley & Sons, New York, 1952).

44) J.R.Grover and J.Gilat: Phys. Rev. 157 (1967) 802.

45) T.Shibata, T.Itahashi and T.Wakatsuki: Proc. Int. Conf. on nuclear physics, Munich, Vol.1, ed. J. de. Boer and H.J.Mang (North-Holland, Amsterdam 1973) p.221.

46) T.Shibata, T.Itahashi and T.Wakatsuki: Nucl. Phys. A237 (1975) 382.

47) S.Matsuki, S.Nakamura, M.Hyakutake, M.Matoba, Y.Yoshida and I.Kumabe: Nucl. Phys. A201 (1973) 608.

48) M.Grecescu, A.Nilsson and Harms-Ringdahl: Nucl. Phys. A212 (1973) 429.

49) V.Sergeev, J.Becker, L.Eriksson, L.Gidefeldt and L.Holmberg: Nucl. Phys. A202 (1973) 385, F.S.Dietrich, B.Herskind, R.A.Naumann, R.G.Stokstad and G.E.Walker: Nucl. Phys. A155 (1970) 209.

Figure captions

Fig.1 Experimental arrangement.

Fig.2 Scattering chambers used in the γ-ray measurements. (a) The beam goes to a Faraday cup through the target chamber. (b) The beam is stopped at the lead sheet in the chamber.

Fig.3 Gamma-ray spectrum obtained from the $^{93}Nb(\alpha,2n\gamma)^{95}Tc$ reaction at 22.5 MeV. Gamma-rays indicated by arrows come from the $^{93}Nb(\alpha,n\gamma)$ reaction.

Fig.3 Corrections for the γ-ray energies. The deviations from the linear function of channel number are shown for the γ-rays from the decay of ^{60}Co, ^{88}Y, ^{133}Ba, ^{137}Cs and ^{228}Th.

Fig.5 Relative efficiency curve for the 30 cc Ge(Li) detector. The γ-rays from the β-decay of ^{133}Ba and ^{152}Eu were measured.

Fig.6 Excitation functions of γ-rays from the $^{93}Nb(\alpha,2n\gamma)$ reaction. Errors shown are only statistical ones.

Fig.7 Excitation function of γ-rays from the $^{93}Nb(\alpha,2n\gamma)^{95}Tc$.

Fig.8 Block diagram of electronics used in the γ-γ coincidence measurements. The number for each circuit is for ORTEC system.

Fig.9-11 Coincidence spectra. Contributions which come from the continuous background in the gate spectra are not subtracted. The γ-rays indicated by an asterisk have large coincidence rate (>60 %), and these γ-rays were used to constract the level scheme.

Fig.12 Block digarams for delayed γ-ray measurements.

(a) Gamma ray spectra were accmulated at different time intervals from the beam burst in this system. (b) Decay curves for some transition were measured by this system.

Fig.13 (a) Circuit diagram to pick up the cyclotron R-F signal. (b) Filter tuned to cyclotron R-F signal.

Fig.14 Angular distributions of γ-rays from the $^{93}Nb(\alpha,2n\gamma)^{95}Tc$ reaction. Gamma spectra were measured twice at each angle (three times at 90°).

Fig.15 Angular distributions of γ-rays from the $^{93}Nb(\alpha,2n\gamma)^{95}Tc$ reaction.

Fig.16 Attenuation of alignment of the compound nuclei with spin J_c produced by capture of the α-particle.

Fig.17 Attenuation coefficients α_2 obtained from angular distributions of γ-rays following the (α,2n) reaction. The values for the target spin 5/2 and 7/2 are obtained from the results in ref.22-26. Values for the target spin 9/2 are obtained from the present work. The solid curve is the attenuation coefficients calculated from eq.2.6 for the target spin 9/2. The dashed curve represent the calculations for the target spin zero.

Fig.18 Proposed level scheme for ^{95}Tc.

Fig.19 Parametric representation of A_2^{max}/A_0 and A_4^{max}/A_0 for the 337 keV, 882 keV and the 957 keV transitions. Attenuation coefficients α_2 for the 337, 882 and 957 keV transitions are estimated to be 0.29±0.1, 0.51±0.1

and 0.45±0.1 from fig.17, respectively. The attenuation coefficients α_4 were obtained under the assumption of a Gaussian distribution of substates.[19]

Fig.20 The core multiplets in ^{93}Nb and ^{95}Tc caused by the coupling of 1g 9/2 proton to the 1st 2^+ state of the core. The results for ^{92}Zr, ^{93}Nb, ^{94}Mo and ^{96}Ru are give in ref.40, 31-32, 5 and 29. and 41, respectively.

Fig.21 Energies of the multiplet states expected from the simple vibration where the diagonal elements for the $Q_c^{(2)}$ operater vanish.

Fig.22 Diagonal element and phonon energy of the core obtained so as to reproduce the 11/2 and 13/2 states in the multiplet in ^{95}Tc.

Fig.23 Energies of the core multiplet states in ^{95}Tc. The 11/2 and 13/2 states are adjusted to the experiment.

Fig.24 (A); Energies of the core multiplet states for the value of χ=2.7 keV fm^{-4} (see Text).

(B); The level structure calculated by using the pairing + QQ - force. The strength of the QQ-force was adjusted so as to reproduce the excitation energy of the 7/2 state.[38]

(C); The level structure obtained by taking into account the 1g 7/2 and 2d 5/2 single proton orbits in the upper major shell too.

Fig.25 Diagonal element and phonon energy of the core obtained to reproduce the 11/2 and 13/2 states in the multiplet

in ^{93}Nb.

Fig.26 Energies of the core multiplet states in ^{93}Nb. The energies of 11/2 and 13/2 states are adjusted to the experiment.

Fig.27 Average neutron momentum carried away by neutron evaporation.

Fig.28 Transmission coefficients for various neutron energy.

Table 1. Gamma-Ray Energies, Relative Intensities and Coefficients of Angular Distribution

E_γ	I_γ	A_2/A_0	A_4/A_0
151.8 ± 0.2	0.6 ± 0.10		
290.6 ± 0.2	0.8 ± 0.1	-0.10 ± 0.16	-0.16 ± 0.19
301.2 ± 0.3	0.6 ± 0.2	-0.09 ± 0.13	+0.02 ± 0.15
305.7 ± 0.2	1.1 ± 0.2	+0.21 ± 0.12	+0.03 ± 0.14
336.6 ± 0.2	20.8 ± 1.2	-0.147±0.026	-0.027±0.028
348.1 ± 0.2	1.3 ± 0.2	-0.48 ± 0.16	+0.21 ± 0.18
363.3 ± 0.2	14.1 ± 0.8	-0.20 ± 0.03	-0.03 ± 0.05
385.4 ± 0.2	2.0 ± 0.5	-0.01 ± 0.10	-0.17 ± 0.13
402.4 ± 0.2	5.1 ± 0.4	+0.32 ± 0.04	-0.08 ± 0.05
546.8 ± 0.2	10.4 ± 0.7	+0.18 ± 0.03	-0.04 ± 0.04
592.5 ± 0.2	20.1 ± 1.1	+0.176±0.021	-0.042±0.025
607.9 ± 0.3	2.2 ± 0.5	-0.09 ± 0.08	-0.01 ± 0.10
613.9 ± 0.2	2.2 ± 0.5	-0.20 ± 0.15	+0.13 ± 0.17
626.9 ± 0.4	4.2 ± 0.9		
629.0 ± 0.2	20.9 ± 1.2	+0.12 ± 0.03	-0.03 ± 0.03
633.1 ± 0.2	67.1 ± 3.5	+0.236±0.022	-0.055±0.024
663.6 ± 0.2	19.7 ± 1.1	-0.11 ± 0.03	+0.01 ± 0.03
667.2 ± 0.2	16.5 ± 1.8	+0.30 ± 0.02	+0.03 ± 0.02
668.7 ± 0.2	17.8 ± 1.9		
716.7 ± 0.2	3.2 ± 0.4	+0.35 ± 0.08	-0.11 ± 0.10
723.0 ± 0.3	3.1 ± 0.5	-0.06 ± 0.05	-0.14 ± 0.07
745.1 ± 0.2	7.4 ± 0.6	-0.21 ± 0.05	-0.03 ± 0.06
748.8 ± 0.3	2.2 ± 0.4	-0.05 ± 0.10	-0.14 ± 0.12

Table 1. (continued)

E_γ	I_γ	A_2/A_0	A_4/A_0
797.9 ± 0.2	6.4 ± 0.5	+0.20 ± 0.05	-0.11 ± 0.06
811.0 ± 0.3	12.2 ± 0.8	+0.41 ± 0.05	-0.12 ± 0.03
878.6 ± 0.2	6.1 ± 0.9	-0.08 ± 0.03	+0.02 ± 0.04
882.4 ± 0.2	100.0 ± 5.1	+0.217±0.018	-0.051±0.021
957.3 ± 0.2	36.4 ± 1.8	-0.339±0.016	+0.067±0.018
969.1 ± 0.2	10.8 ± 0.7	+0.30 ± 0.04	-0.13 ± 0.04
1031.9 ± 0.2	9.3 ± 0.6	+0.24 ± 0.06	-0.06 ± 0.07
1179.0 ± 0.3	1.2 ± 0.3	-0.19 ± 0.24	+0.37 ± 0.37
1214.7 ± 0.3	2.6 ± 0.6	+0.19 ± 0.08	-0.02 ± 0.10
1237.5 ± 0.3	3.0 ± 0.5	-0.34 ± 0.05	-0.01 ± 0.06
1264.5 ± 1.0	1.3 ± 0.5	-0.11 ± 0.20	+0.26 ± 0.24
1307.5 ± 0.2	4.7 ± 0.5	-0.25 ± 0.06	-0.06 ± 0.06
1407.7 ± 0.6	2.0 ± 0.4	+0.09 ± 0.07	+0.15 ± 0.09
1524.5 ± 0.6	2.2 ± 0.4	-0.03 ± 0.09	-0.06 ± 0.11
1646.8 ± 0.6	2.2 ± 0.5	-0.22 ± 0.10	-0.11 ± 0.11
1695.8 ± 1.0	2.0 ± 0.7	-0.02 ± 0.10	-0.02 ± 0.12
1846.6 ± 0.6	4.1 ± 0.9		

The relative intensities were obtained from the γ-ray spectrum at 55° to the beam direction.

Table 2. Relative Intensities and Relative Coincidence Rate** in Gamma-Gamma Coincidence Spectra

Gate / E_γ	337	363	593	629	633	664	667 +669	882	957
291	15±2 (148±43)								
301	14±2 (326±219)								
337				52±20 (27±11)				10±3 (29±9)	20±12 (25±14)
363				37±18 (29±14)	25±4 (158±22)		32±5 (142±33)	10±3 (42±14)	
402		17±7 (199±80)			7±4 (110±69)			6±4 (74±51)	
547				100±35 (100±36)*					
593		19±7 (67±25)			15±6 (76±29)	38±27 (75±53)			100±20 (100±21)
633		100±13 (100±13)*	26±15 (15±9)			92±32 (52±18)	100±14 (100±15)*	100±6 (100±6)*	49±20 (14±6)
664			51±19 (96±36)				18±10 (58±32)	19±6 (63±19)	35±21 (33±20)
667 +669		59±14 (125±29)			41±6 (122±18)	40±22 (47±26)		34±4 (72±9)	
745									40±16 (115±48)
749	36±15 (108±62)								

Table 2. (continued)

Gate / E_γ	337	363	593	629	633	664	667 +669	882	957
811			41±28 (161±111)			58±27 (227±110)	18±11 (128±77)		33±14 (65±29)
879	100±18 (100±20)*								
882		78±10 (55±7)		136±30 (17±4)	100±6 (100±6)*	96±31 (38±12)	90±12 (63±9)		39±16 (8±3)
957		27±8 (48±14)	100±16 (100±16)*		12±6 (29±14)	100±19 (100±19)*			
969		36±8 (248±60)			11±6 (106±56)				
1031		13±9 (106±70)			16±8 (176±95)				

** Parentheses show the relative coincidence rate.

The relative coincidence rates were obtained under the assumption that the γ-ray indicated by an asterisk in each column was in coincidence with the γ-ray, on whose photo peak the coincidence gate were set, of 100 % coincidence rate.

The errors do not include the effect of the angular correlation of γ-rays.

Table 3

Matrix Elements and B(E2) Values

	$\lvert\langle\lambda N \lVert Q \rVert \lambda' N'\rangle\rvert^2$ (fm^4)	Coulomb excitation	eq.3.1.[b]
^{94}Mo[a]	$\lvert\langle 21 \lVert Q \rVert 00\rangle\rvert^2$	2180 ± 110	2180[b]
	$\lvert\langle 42 \lVert Q \rVert 21\rangle\rvert^2$	6000 ± 900	7848
	$\lvert\langle 22 \lVert Q \rVert 21\rangle\rvert^2$	5800 ± 130	4362
	$\lvert\langle 02 \lVert Q \rVert 21\rangle\rvert^2$		872
	$\lvert\langle 22 \lVert Q \rVert 00\rangle\rvert^2$	32 ± 7	0

	B(E2) (e^{2}fm^4)	Coulomb excitation	eq.3.3
^{93}Nb[c]	B(E2 9/2 → 13/2)	230 ± 12	221
	B(E2 9/2 → 11/2)	172 ± 9	190
	B(E2 9/2 → 9/2)	26 ± 2	158
	B(E2 9/2 → 9/2')	39 ± 3	
	B(E2 9/2 → 7/2)	168 ± 8	126
	B(E2 9/2 → 5/2)	157 ± 7	95
^{92}Zr[d]	B(E2 0 → 2) e^{2}fm^4	790 ± 10	

a) ref. 5) b) Expected values of the phonon model (eq.3.1), where use was made of the value $\lvert\langle 21 \lVert Q \rVert 00\rangle\rvert^2$ obtained from the Coulomb excitation. c) ref. 42) d) ref.32)

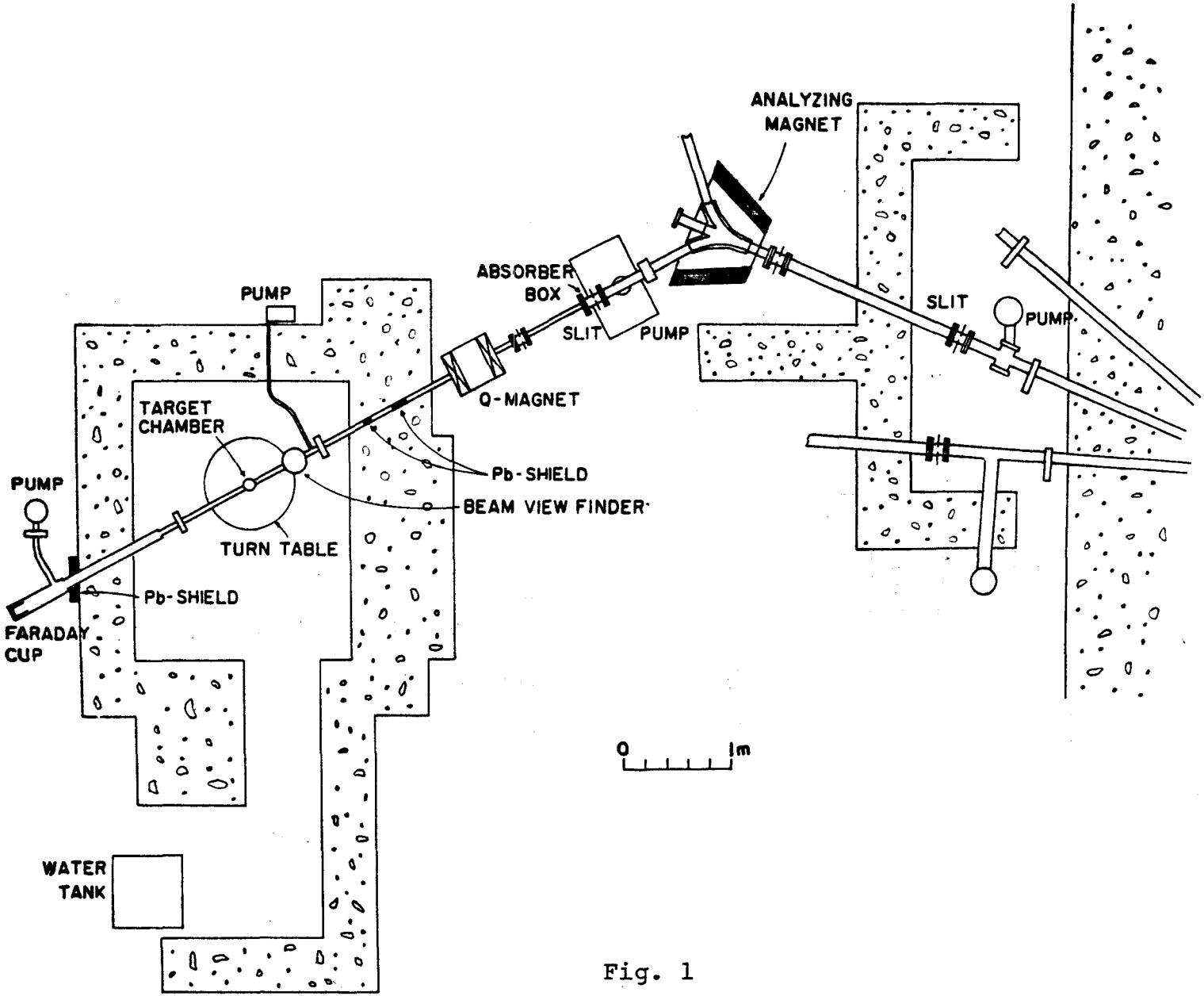
ANALYZING
MAGNET
ABSORBER
BOX
PUMP
SLIT
PUMP
SLIT
PUMP
Q-MAGNET
TARGET
CHAMBER
Pb-SHIELD
BEAM VIEW FINDER
PUMP
TURN TABLE
Pb-SHIELD
FARADAY
CUP
0
1m
WATER
TANK

Fig. 1

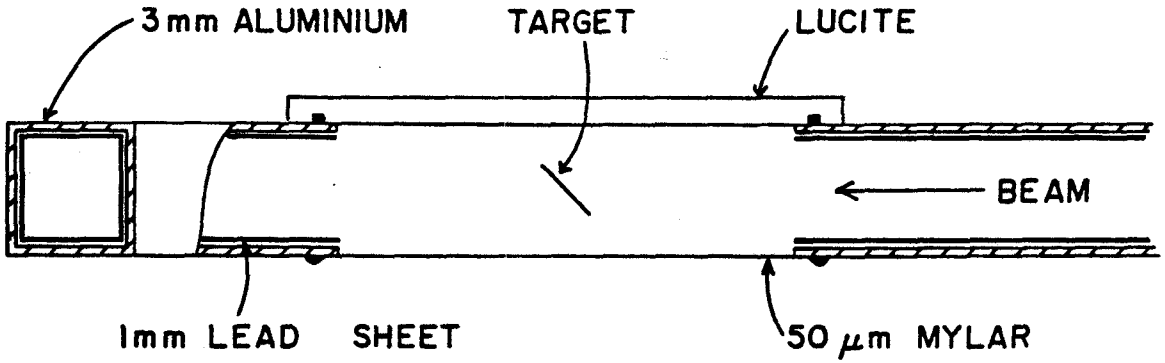
3mm ALUMINIUM
TARGET
LUCITE
BEAM
1mm LEAD SHEET
50 μm MYLAR

(a)

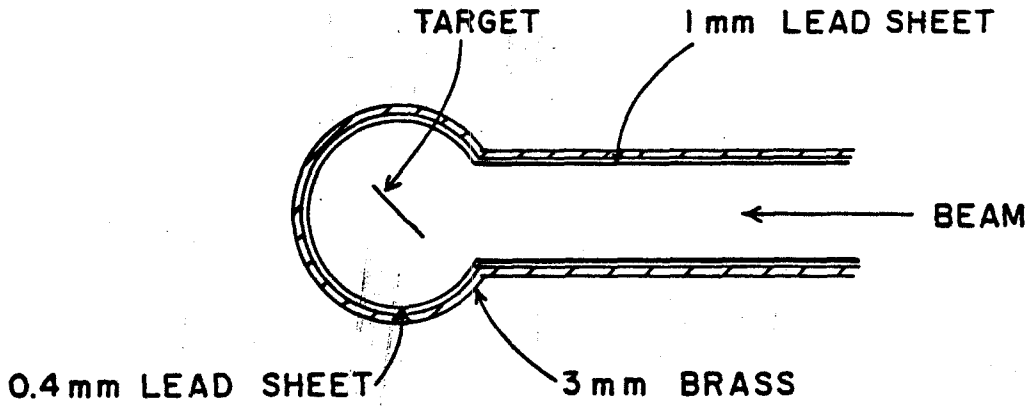
TARGET
1mm LEAD SHEET
BEAM
0.4mm LEAD SHEET
3mm BRASS

(b)

Fig. 2

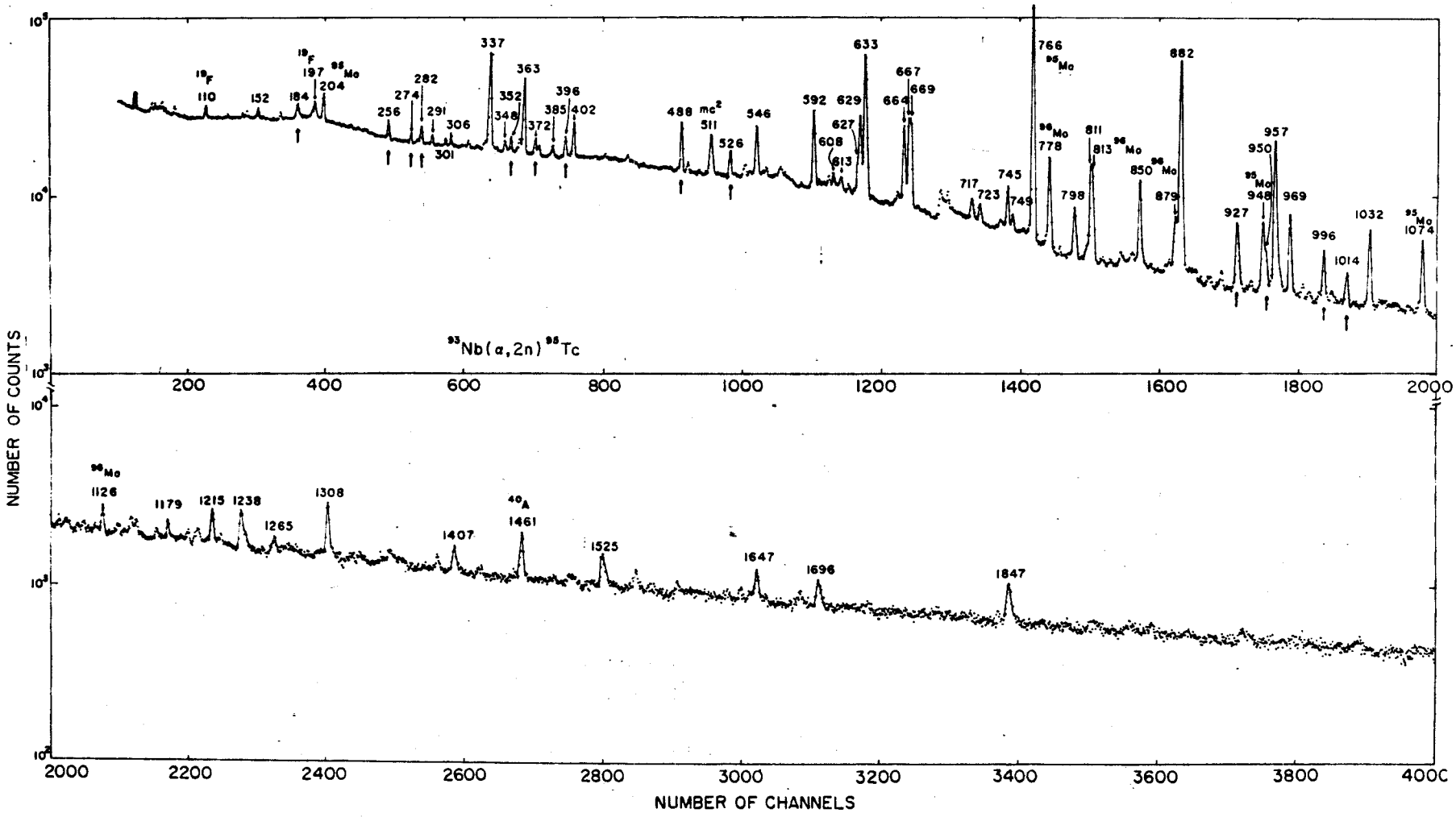
^{93}Nb(α,2n)^{95}Tc
NUMBER OF COUNTS
NUMBER OF CHANNELS
^{19}F 110
152
^{19}F 184
197
^{95}Mo 204
256
274
282
291
301
306
337
348
352
363
372
385
396
402
488
mc^2 511
526
546
592
608
613
627
629
633
664
667
669
717
723
745
749
766
^{95}Mo
^{96}Mo 778
798
811
813
^{96}Mo
850
^{96}Mo
879
882
927
948
^{95}Mo
950
957
969
996
1014
1032
^{95}Mo 1074
^{96}Mo 1126
1179
1215
1238
1265
1308
1407
^{40}A 1461
1525
1647
1696
1847

Fig. 3

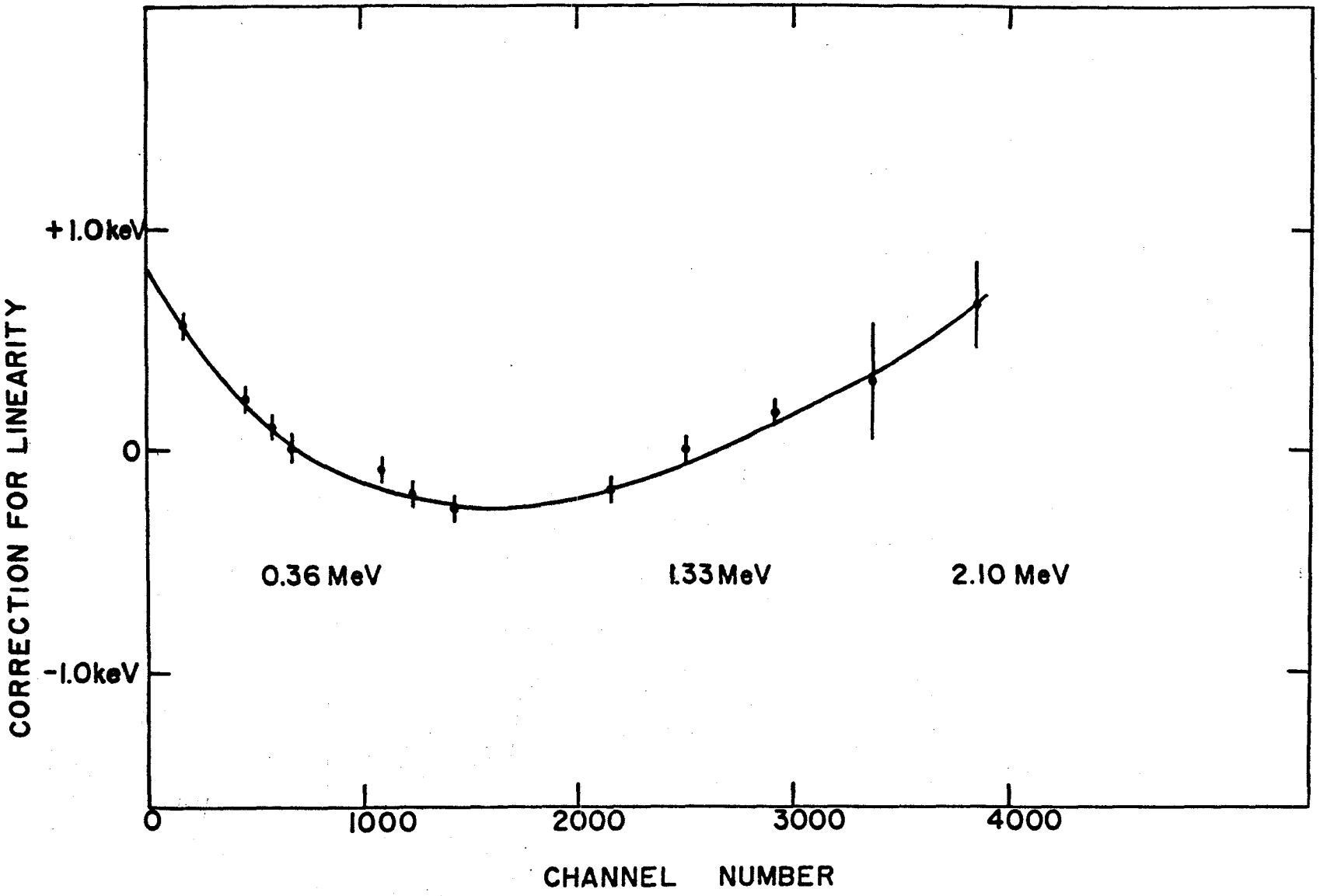
+1.0keV
0
-1.0keV
CORRECTION FOR LINEARITY
0.36 MeV
1.33MeV
2.10 MeV
0
1000
2000
3000
4000
CHANNEL NUMBER

Fig. 4

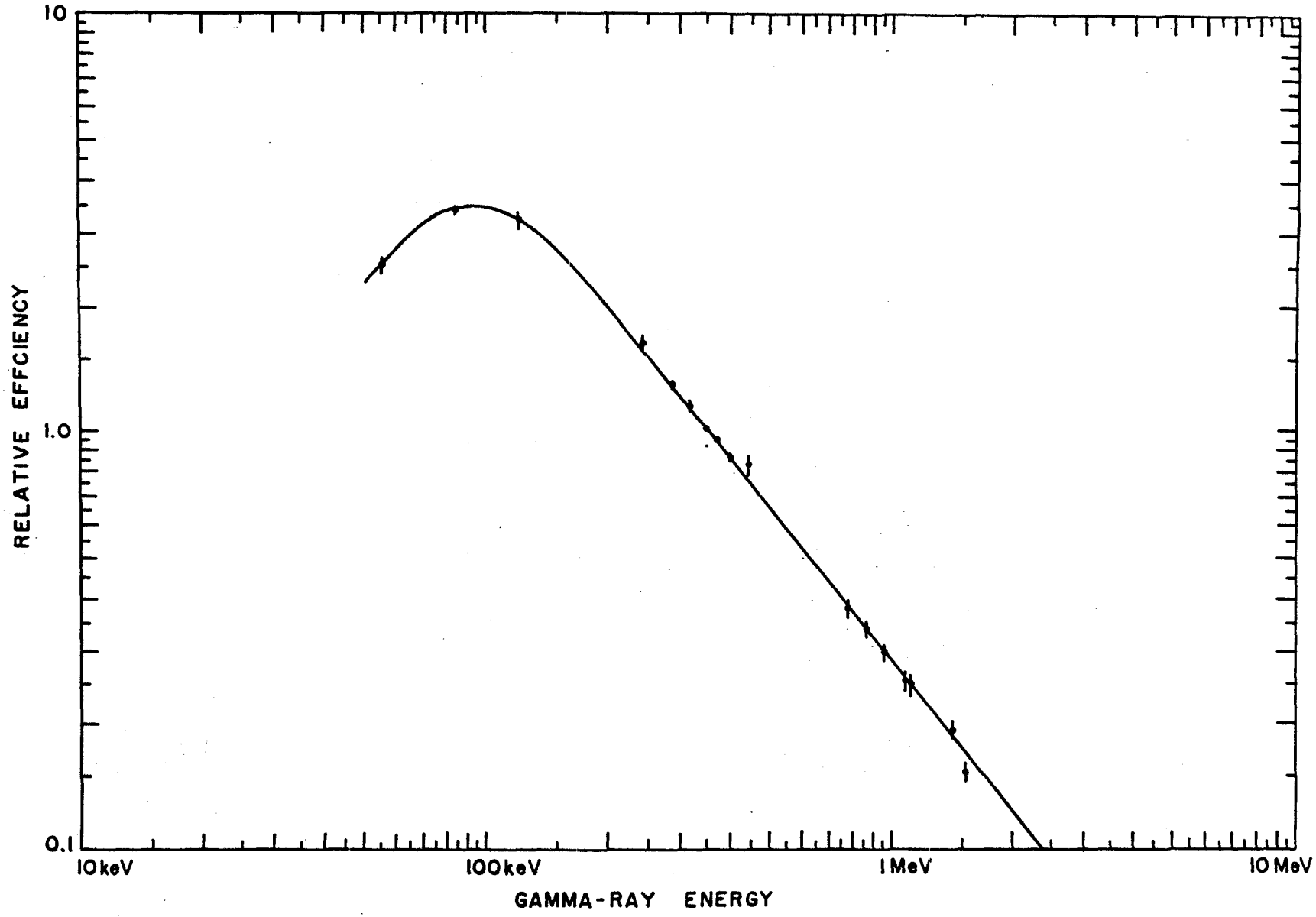
10
1.0
0.1
RELATIVE EFFCIENCY
10keV
100keV
1MeV
10 MeV
GAMMA-RAY ENERGY

Fig. 5

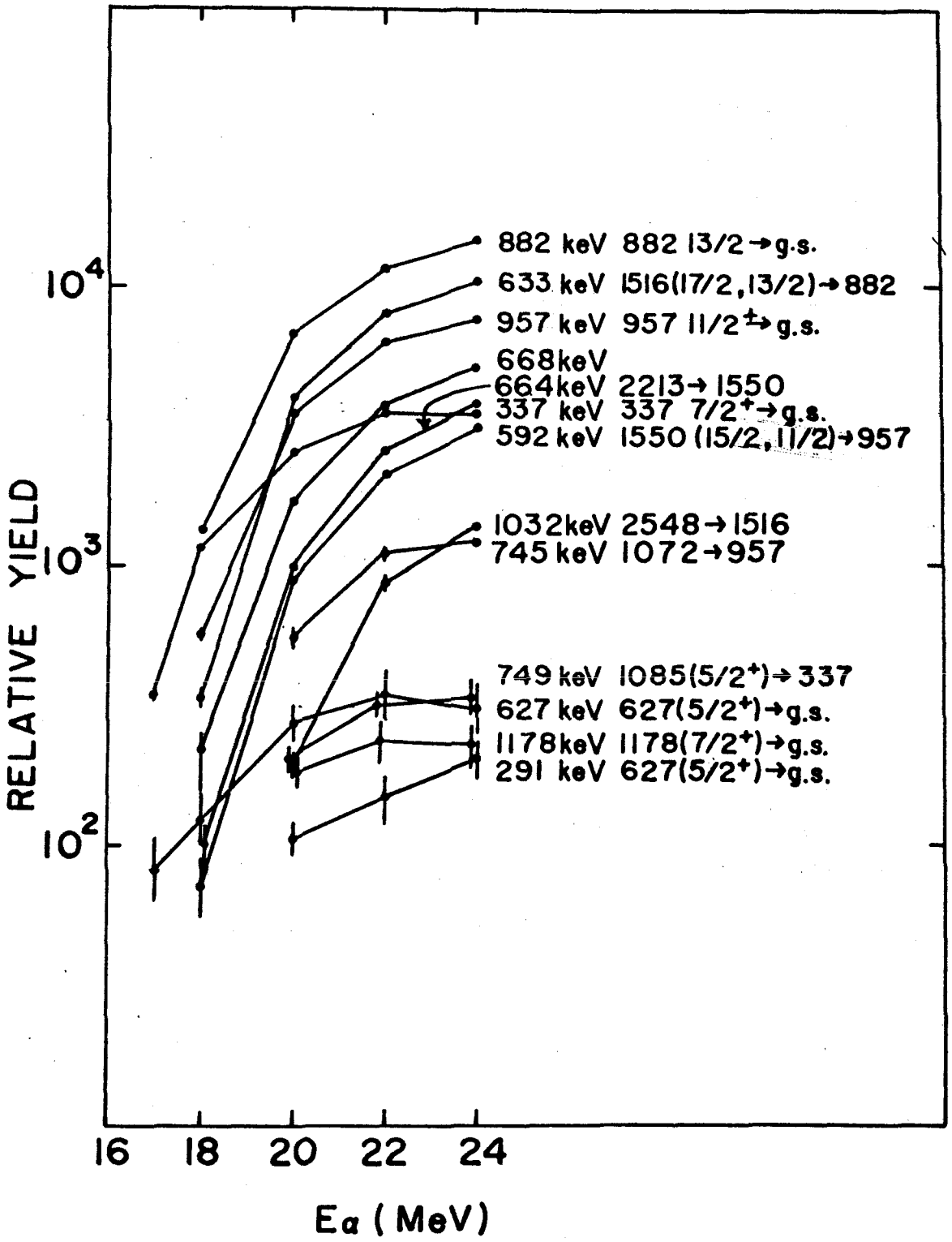
882 keV 882 13/2→g.s.
633 keV 1516(17/2,13/2)→882
957 keV 957 11/2±→g.s.
668keV
664keV 2213→1550
337 keV 337 7/2+→g.s.
592 keV 1550 (15/2,11/2)→957
1032keV 2548→1516
745 keV 1072→957
749 keV 1085(5/2+)→337
627 keV 627(5/2+)→g.s.
1178keV 1178(7/2+)→g.s.
291 keV 627(5/2+)→g.s.
RELATIVE YIELD
10⁴
10³
10²
16
18
20
22
24
Eα (MeV)

Fig. 6

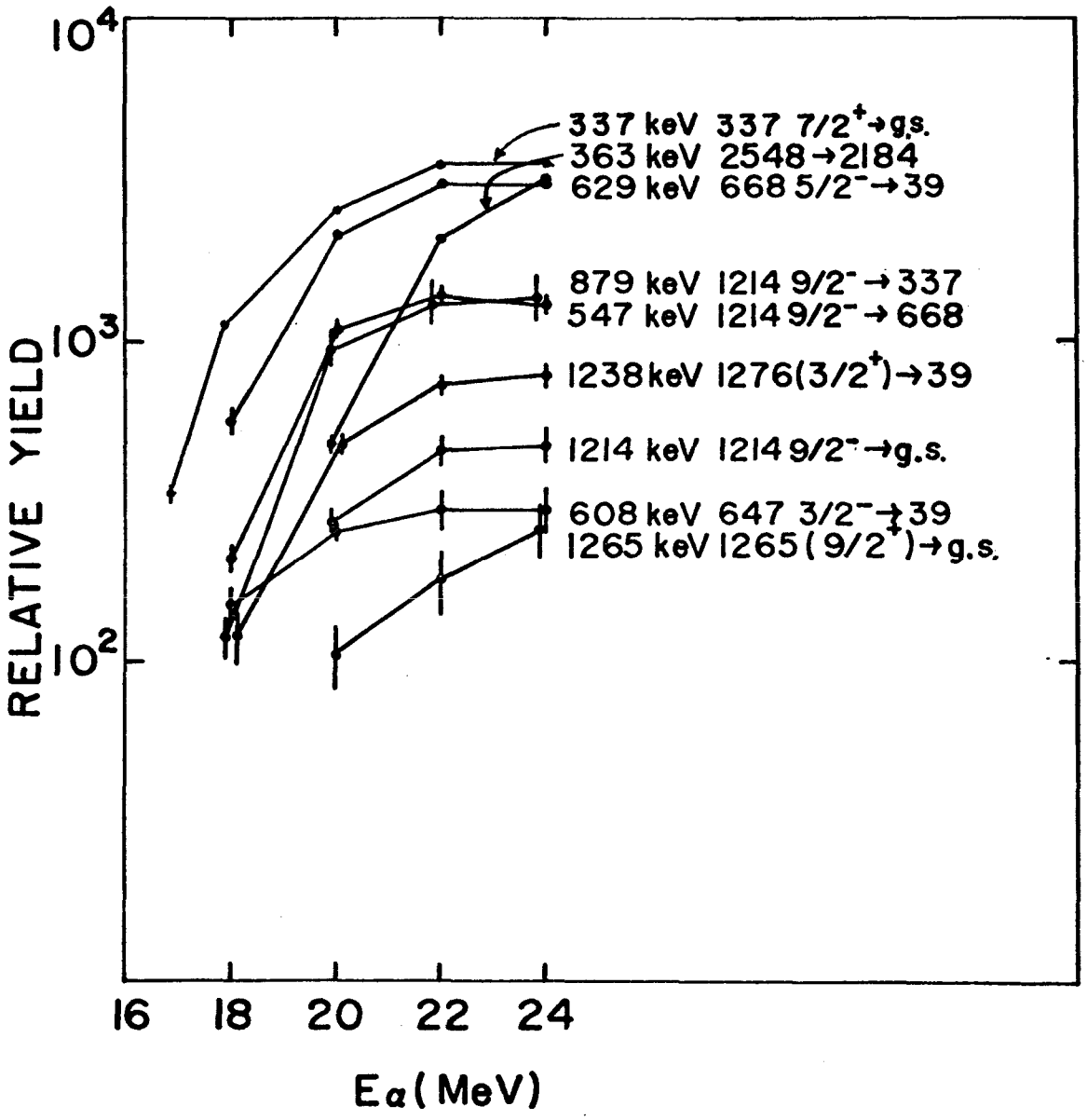
RELATIVE YIELD
10^4
10^3
10^2
337 keV 337 7/2+→g.s.
363 keV 2548→2184
629 keV 668 5/2-→39
879 keV 1214 9/2-→337
547 keV 1214 9/2-→668
1238 keV 1276(3/2+)→39
1214 keV 1214 9/2-→g.s.
608 keV 647 3/2-→39
1265 keV 1265(9/2+)→g.s.
16
18
20
22
24
Eα(MeV)

Fig. 7

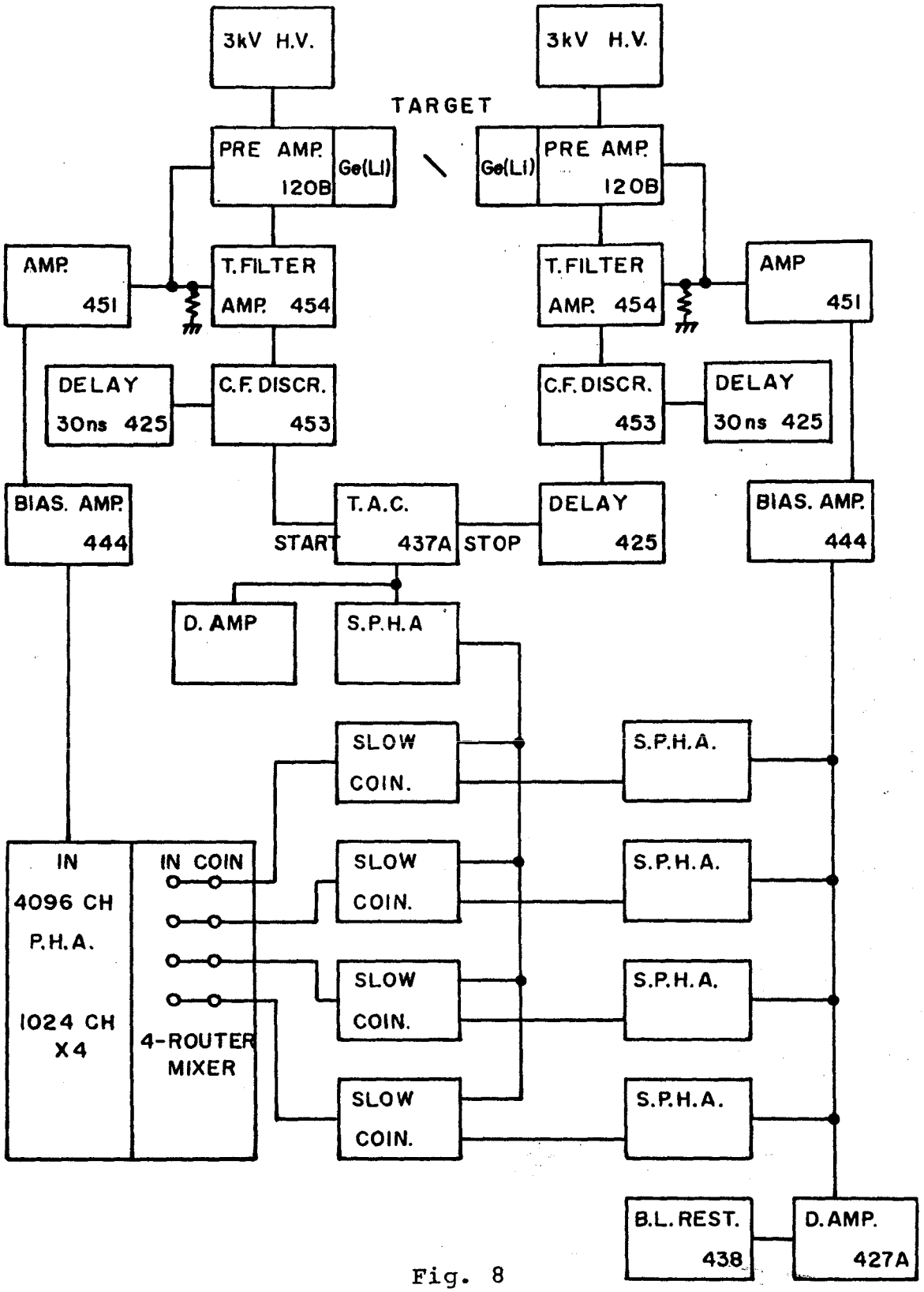
3kV H.V.
3kV H.V.
TARGET
PRE AMP. 120B
Ge(LI)
Ge(LI)
PRE AMP. 120B
AMP. 451
T.FILTER AMP. 454
T.FILTER AMP. 454
AMP 451
DELAY 30ns 425
C.F. DISCR. 453
C.F. DISCR. 453
DELAY 30ns 425
BIAS. AMP. 444
T.A.C. 437A
START
STOP
DELAY 425
BIAS. AMP. 444
D. AMP
S.P.H.A
SLOW COIN.
S.P.H.A.
IN 4096 CH P.H.A. 1024 CH X4
IN COIN
4-ROUTER MIXER
SLOW COIN.
S.P.H.A.
SLOW COIN.
S.P.H.A.
SLOW COIN.
S.P.H.A.
B.L. REST. 438
D.AMP. 427A

Fig. 8

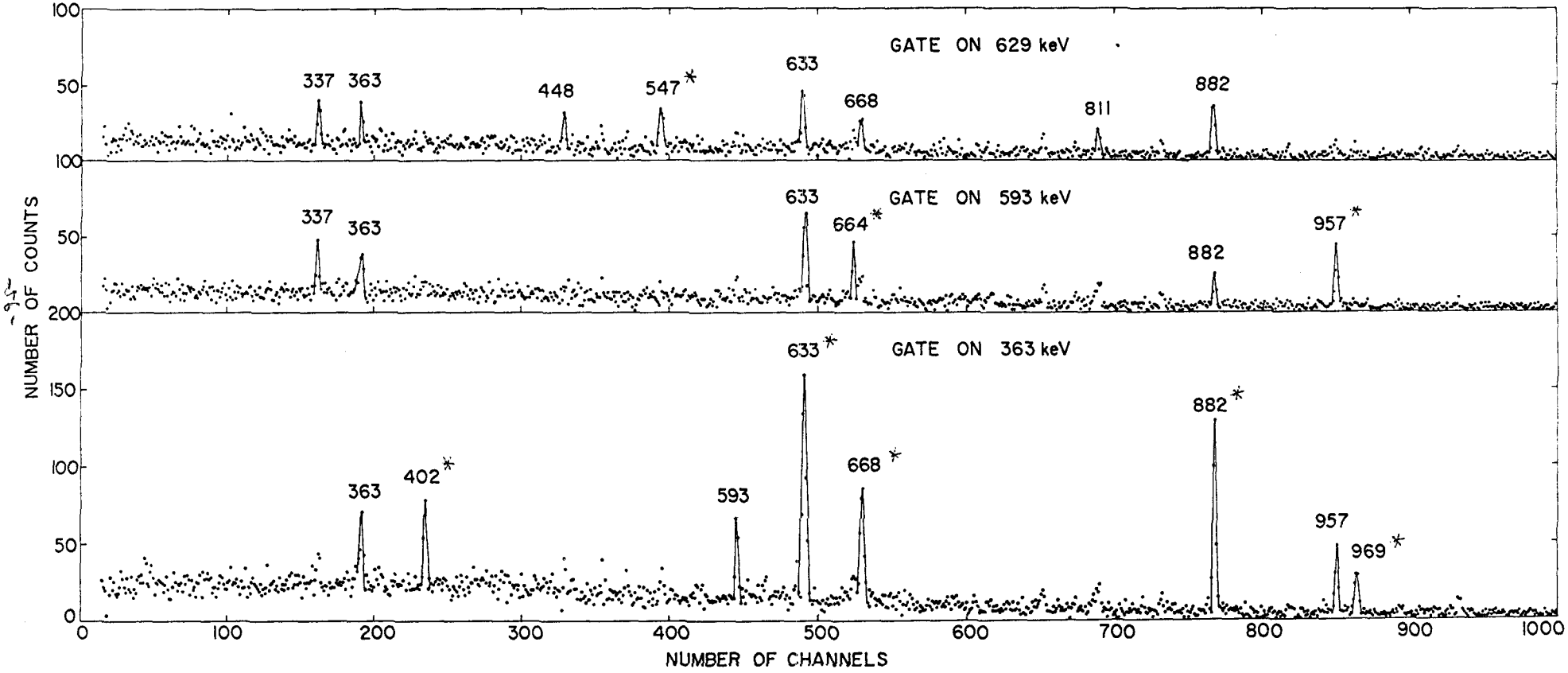
GATE ON 629 keV
337
363
448
547*
633
668
811
882
GATE ON 593 keV
337
363
633
664*
882
957*
GATE ON 363 keV
633*
363
402*
593
668*
882*
957
969*
NUMBER OF COUNTS
NUMBER OF CHANNELS
0
100
200
300
400
500
600
700
800
900
1000
50
150

Fig. 9

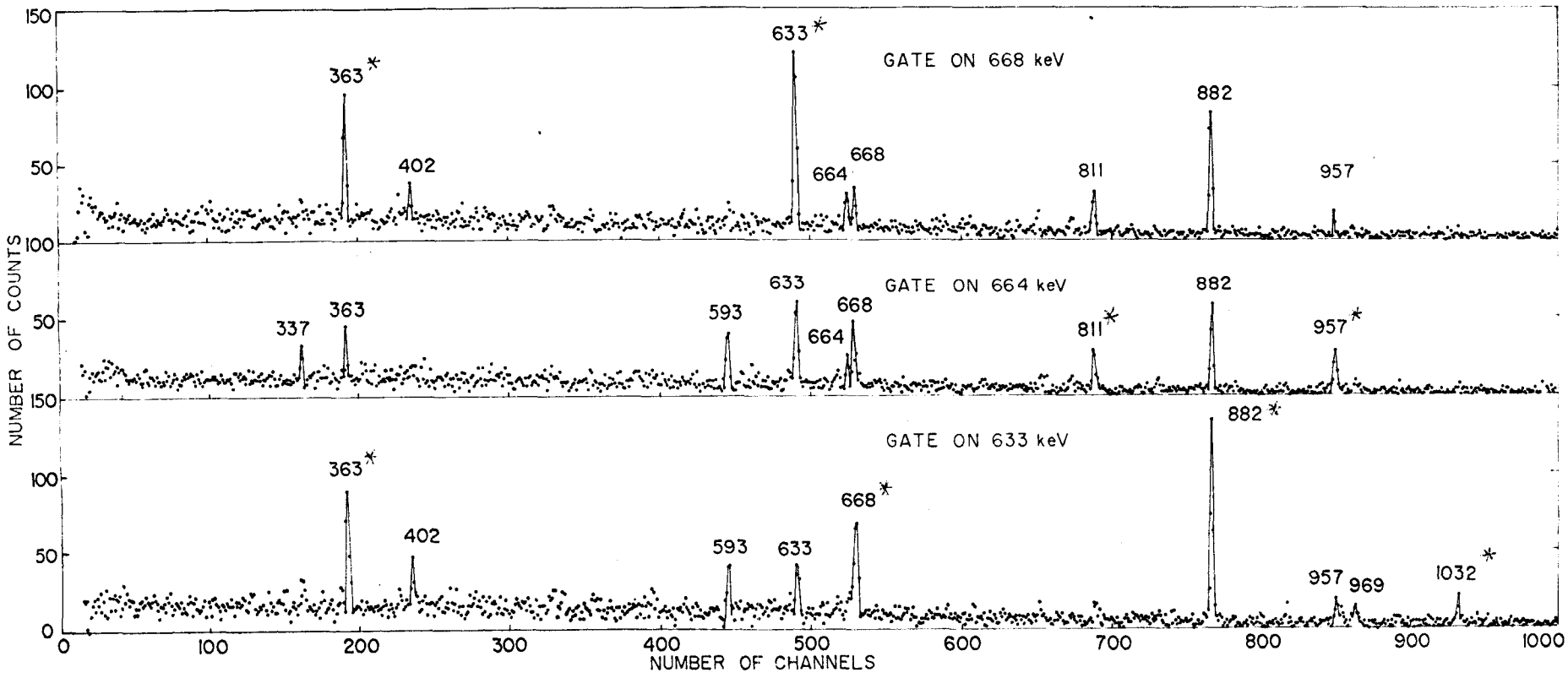
GATE ON 668 keV
363*
633*
402
664
668
811
882
957
GATE ON 664 keV
337
363
593
633
664
668
811*
882
957*
GATE ON 633 keV
363*
402
593
633
668*
882*
957
969
1032*
NUMBER OF COUNTS
NUMBER OF CHANNELS
0
50
100
150
200
300
400
500
600
700
800
900
1000

Fig. 10

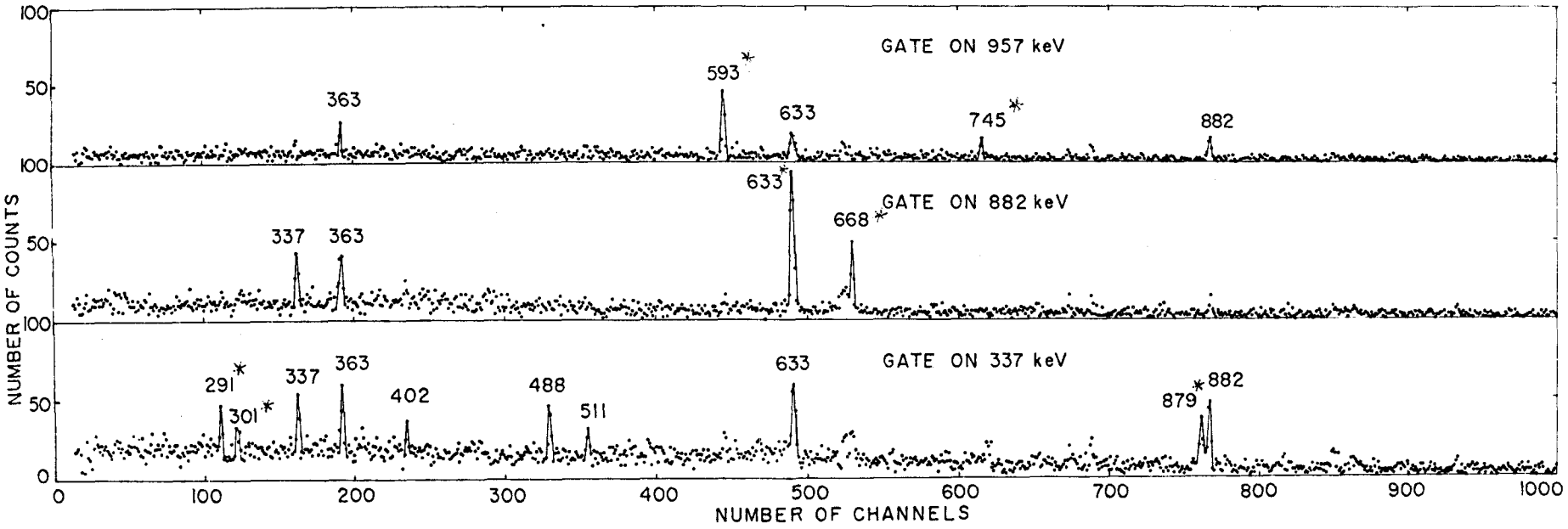
GATE ON 957 keV
363
593*
633
745*
882
GATE ON 882 keV
337
363
633*
668*
GATE ON 337 keV
291*
301*
337
363
402
488
511
633
879
882*
NUMBER OF COUNTS
NUMBER OF CHANNELS
0
50
100
100
200
300
400
500
600
700
800
900
1000

Fig.11

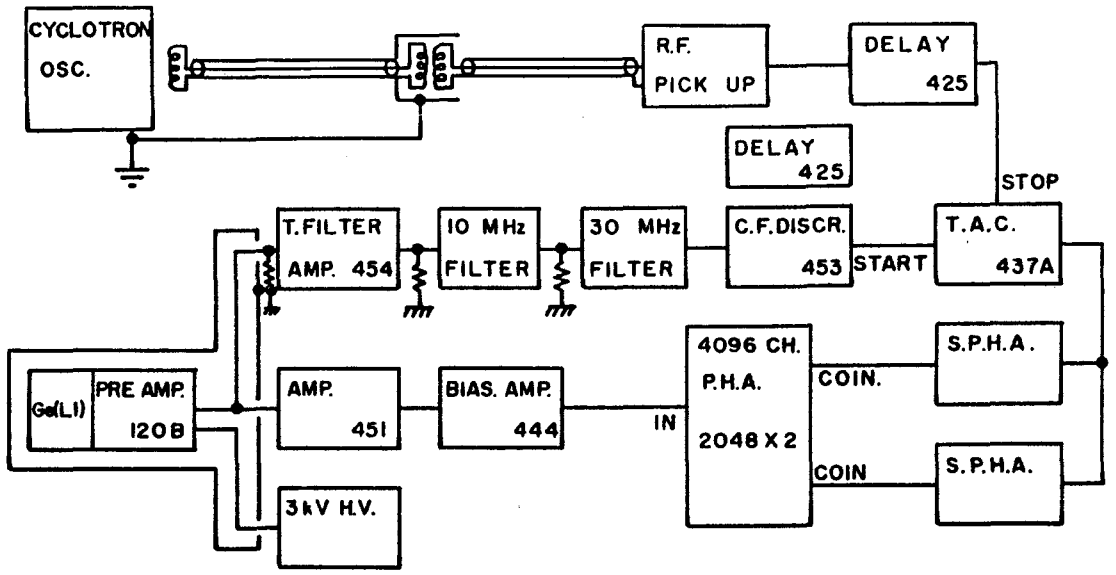
CYCLOTRON
OSC.
R.F.
PICK UP
DELAY
425
DELAY
425
STOP
T.FILTER
AMP. 454
10 MHz
FILTER
30 MHz
FILTER
C.F.DISCR.
453
START
T.A.C.
437A
Ge(LI)
PRE AMP.
120B
AMP.
451
BIAS. AMP.
444
IN
4096 CH.
P.H.A.
2048 X 2
COIN.
COIN
S.P.H.A.
S.P.H.A.
3kV H.V.

(a)

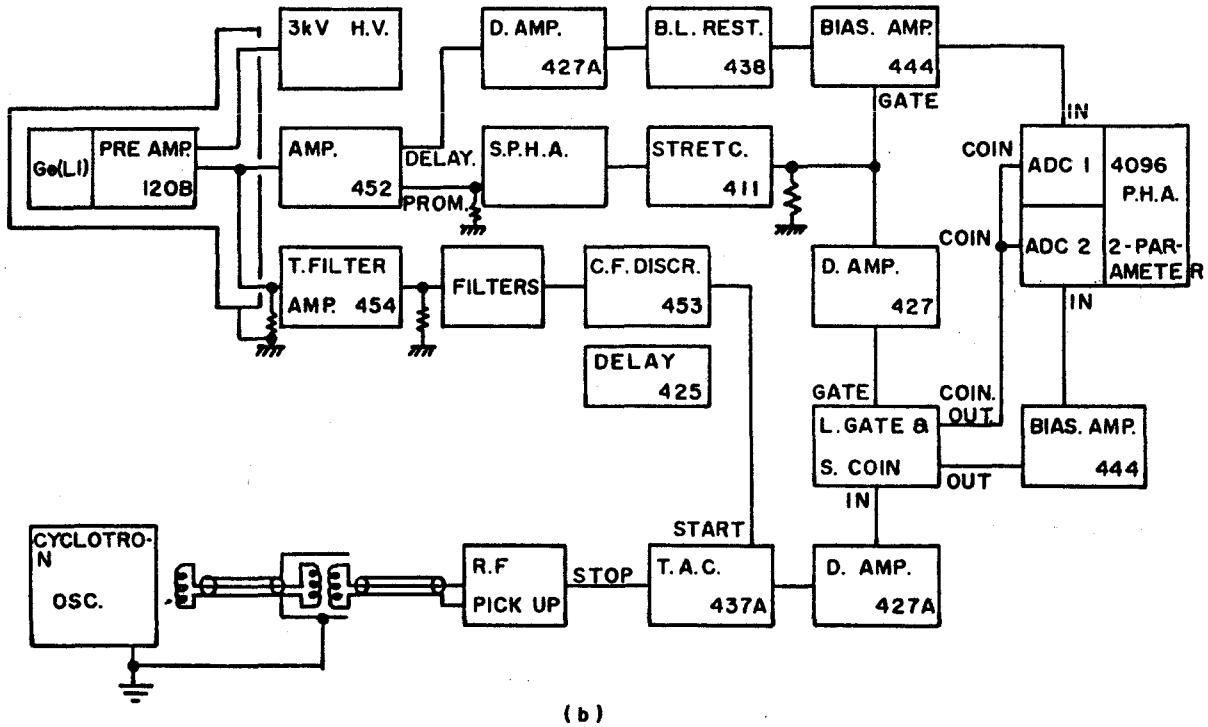
3kV H.V.
D. AMP.
427A
B.L. REST.
438
BIAS. AMP.
444
GATE
IN
Ge(LI)
PRE AMP.
120B
AMP.
452
DELAY.
PROM.
S.P.H.A.
STRETC.
411
COIN
ADC 1
4096
P.H.A.
COIN
ADC 2
2-PAR-
AMETER
IN
T.FILTER
AMP. 454
FILTERS
C.F. DISCR.
453
D. AMP.
427
DELAY
425
GATE
COIN.
OUT
L.GATE &
S. COIN
BIAS. AMP.
444
OUT
IN
START
CYCLOTRON
OSC.
R.F
PICK UP
STOP
T.A.C.
437A
D. AMP.
427A

(b)

Fig. 12

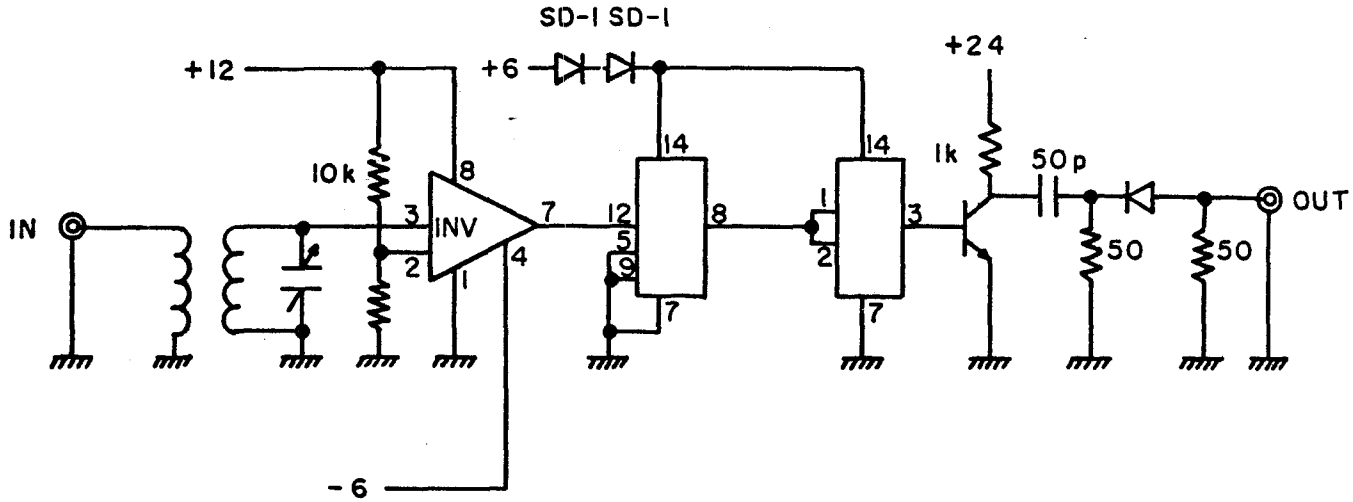
SD-1 SD-1
+12
+6
+24
10k
1k
50p
IN
INV
OUT
50
50
-6
LM306
SN7470
SN7400
IS1516

(a)

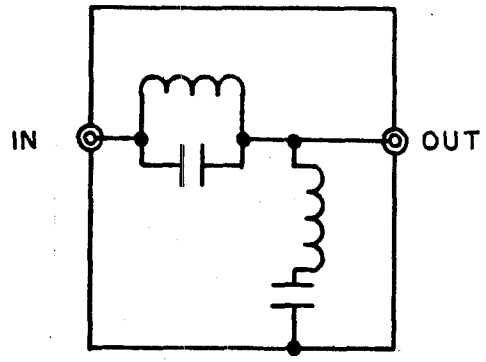
IN
OUT

(b)

Fig. 13

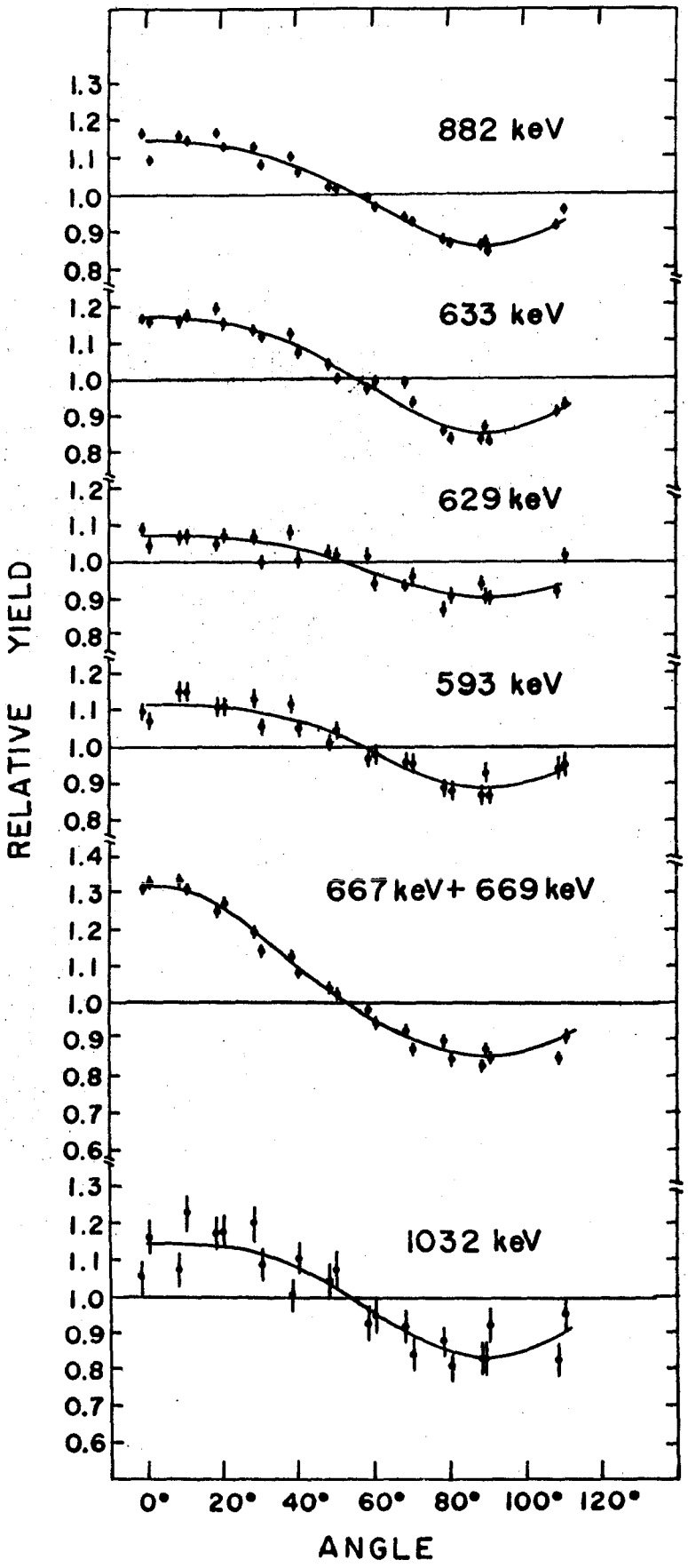
882 keV
633 keV
629 keV
593 keV
667 keV+ 669 keV
1032 keV
RELATIVE YIELD
ANGLE
0°
20°
40°
60°
80°
100°
120°

Fig. 14

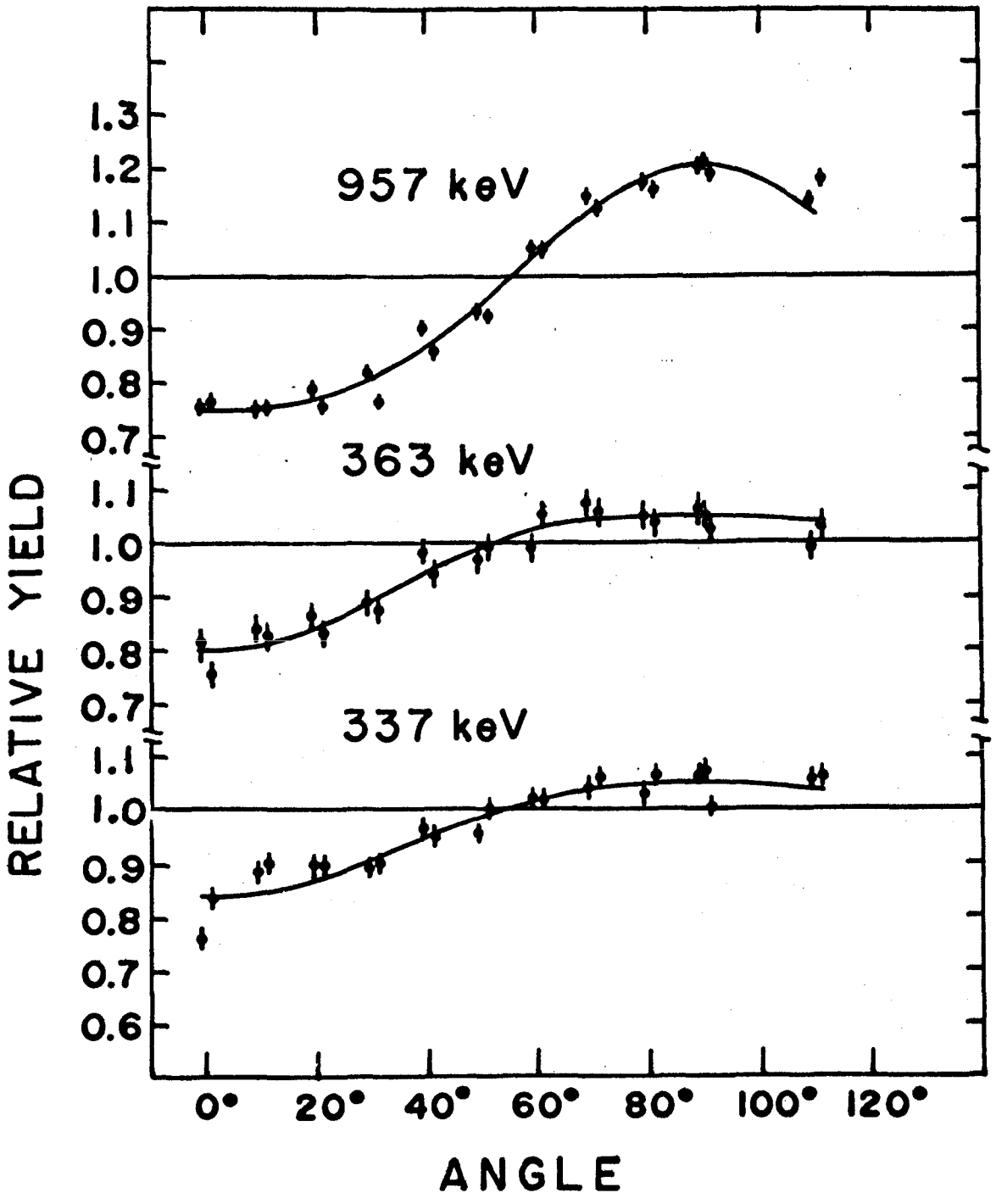
957 keV
363 keV
337 keV
RELATIVE YIELD
ANGLE
1.3
1.2
1.1
1.0
0.9
0.8
0.7
0.6
0°
20°
40°
60°
80°
100°
120°

Fig. 15

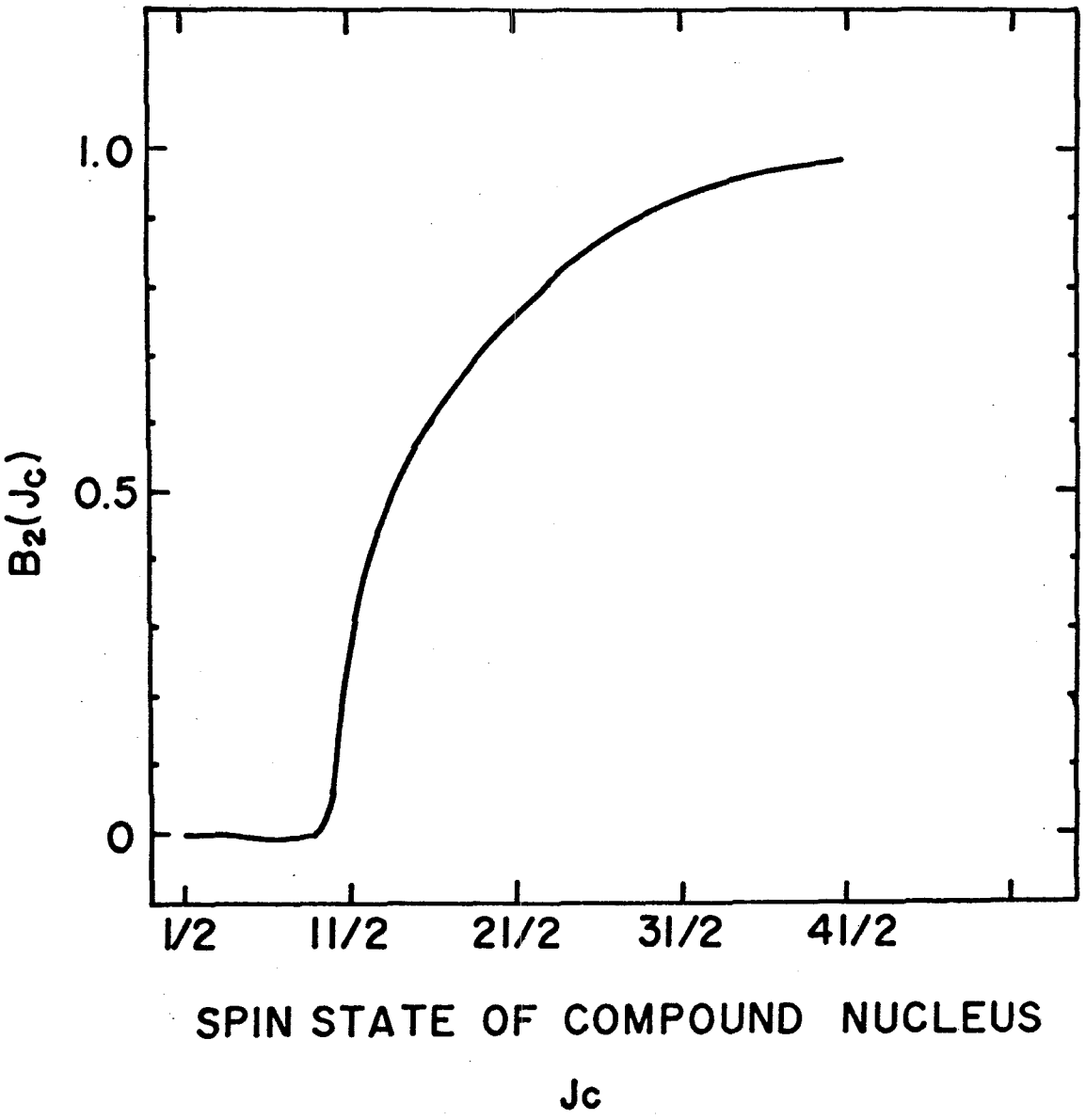
1.0
0.5
0
$B_2(J_c)$
1/2
11/2
21/2
31/2
41/2
SPIN STATE OF COMPOUND NUCLEUS
Jc

Fig. 16

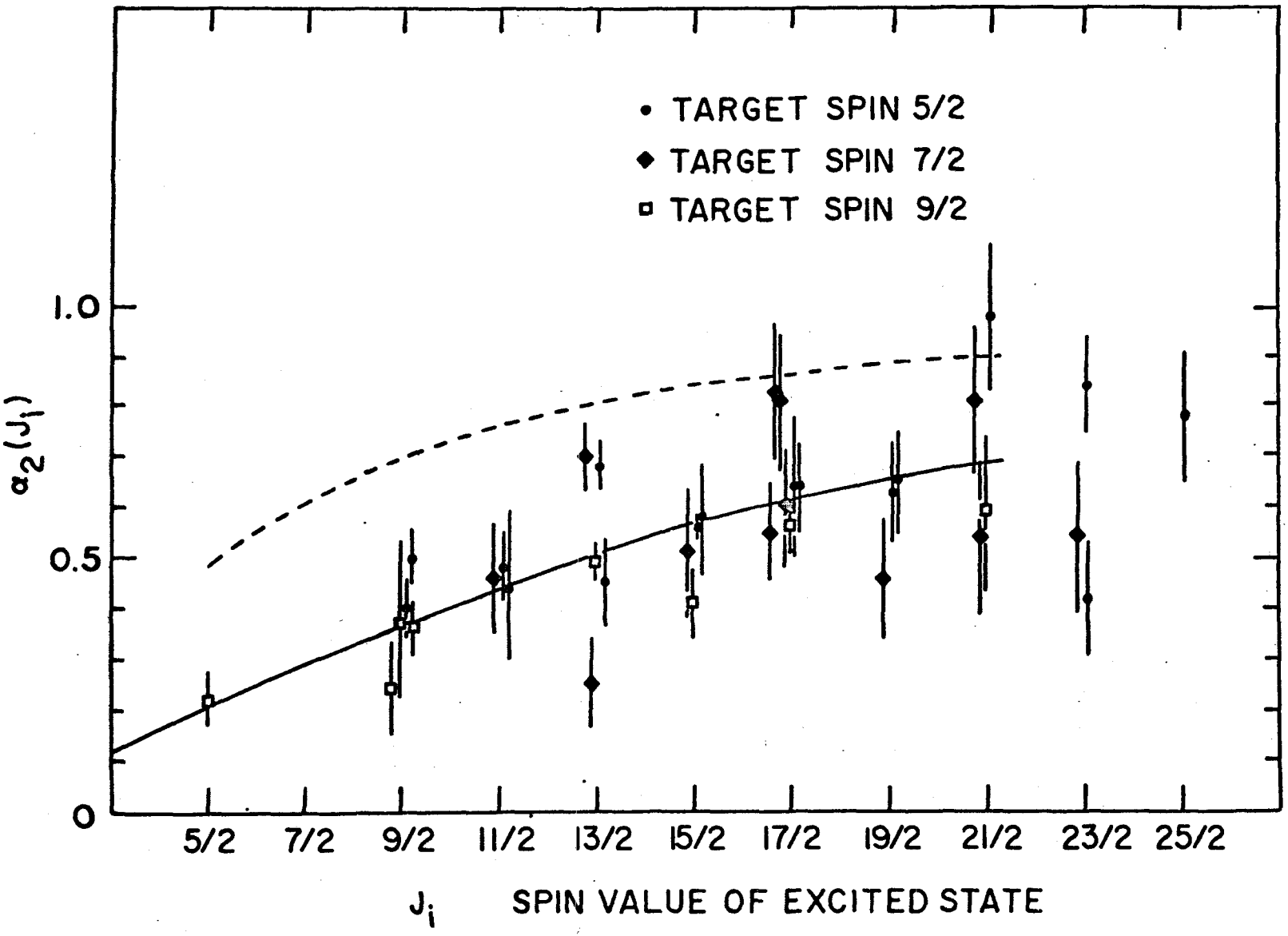
• TARGET SPIN 5/2
◆ TARGET SPIN 7/2
▫ TARGET SPIN 9/2
1.0
0.5
0
$a_2(J_i)$
5/2
7/2
9/2
11/2
13/2
15/2
17/2
19/2
21/2
23/2
25/2
J_i SPIN VALUE OF EXCITED STATE

Fig. 17

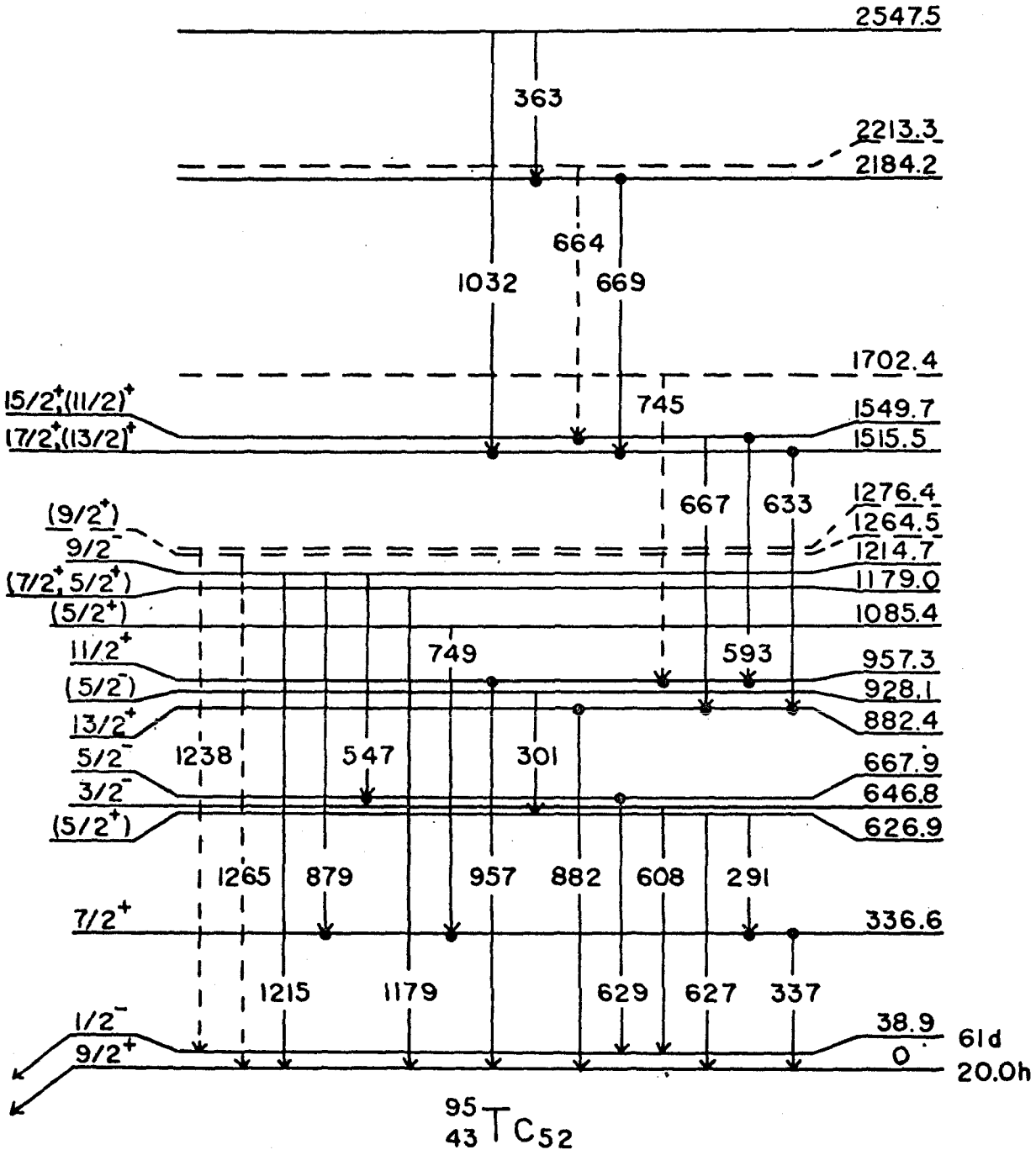
2547.5
363
2213.3
2184.2
664
1032
669
1702.4
15/2+,(11/2)+
17/2+,(13/2)+
745
1549.7
1515.5
667
633
1276.4
(9/2+)
1264.5
9/2-
1214.7
(7/2+,5/2+)
1179.0
(5/2+)
1085.4
11/2+
749
593
957.3
(5/2-)
928.1
13/2+
882.4
5/2-
1238
547
301
667.9
3/2-
646.8
(5/2+)
626.9
1265
879
957
882
608
291
7/2+
336.6
1215
1179
629
627
337
1/2-
38.9
61d
9/2+
0
20.0h
95 43 Tc52

Fig. 18

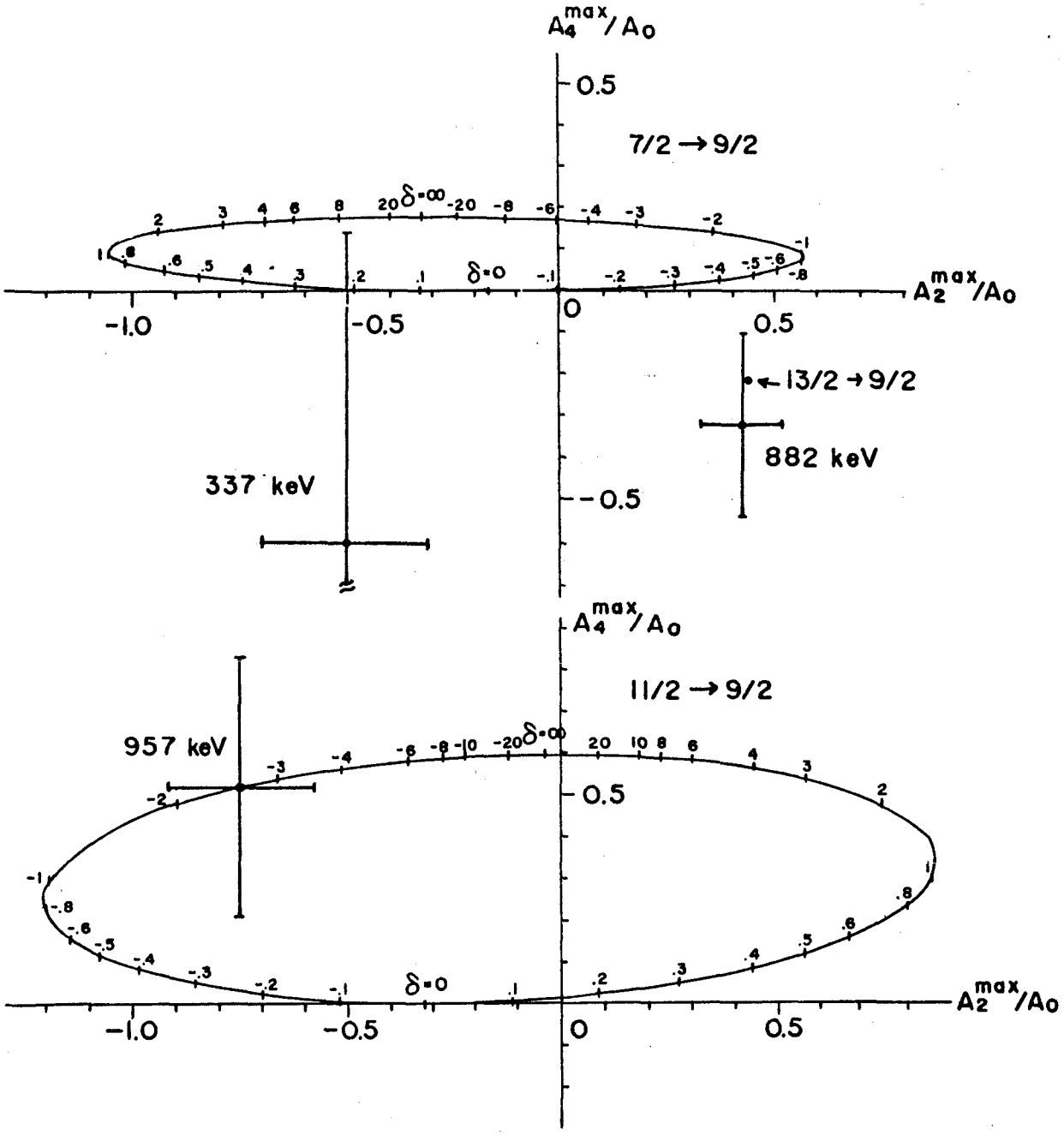
A_4^{max}/A_0
0.5
7/2 → 9/2
δ=∞
δ=0
A_2^{max}/A_0
-1.0
-0.5
0
0.5
← 13/2 → 9/2
882 keV
337 keV
-0.5
A_4^{max}/A_0
11/2 → 9/2
957 keV
δ=∞
0.5
δ=0
A_2^{max}/A_0
-1.0
-0.5
0
0.5

Fig. 19

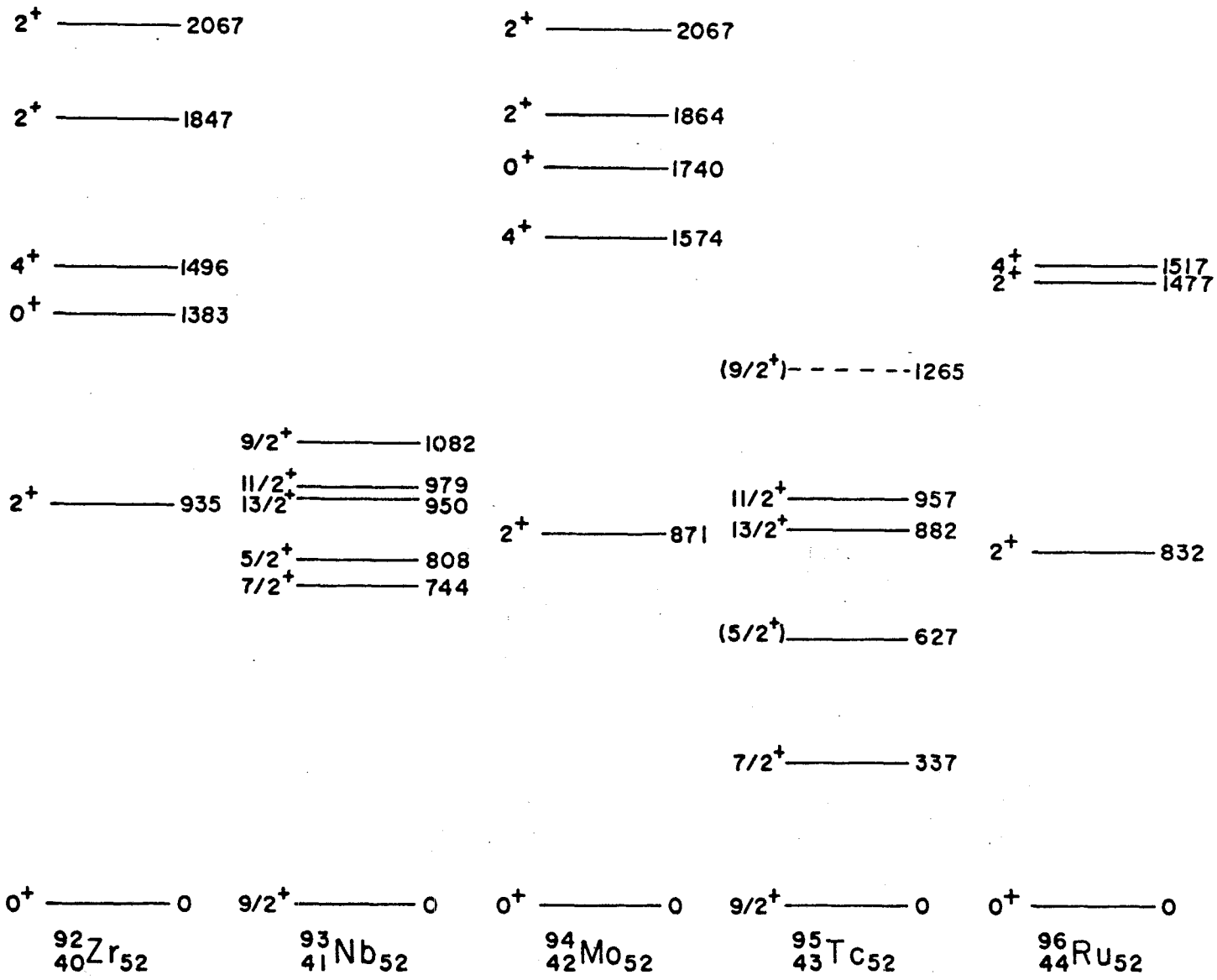
2+ 2067
2+ 1847
4+ 1496
0+ 1383
2+ 935
0+ 0
92 40 Zr52
9/2+ 1082
11/2+ 979
13/2+ 950
5/2+ 808
7/2+ 744
9/2+ 0
93 41 Nb52
2+ 2067
2+ 1864
0+ 1740
4+ 1574
2+ 871
0+ 0
94 42 Mo52
(9/2+) 1265
11/2+ 957
13/2+ 882
(5/2+) 627
7/2+ 337
9/2+ 0
95 43 Tc52
4+ 1517
2+ 1477
2+ 832
0+ 0
96 44 Ru52

Fig. 20

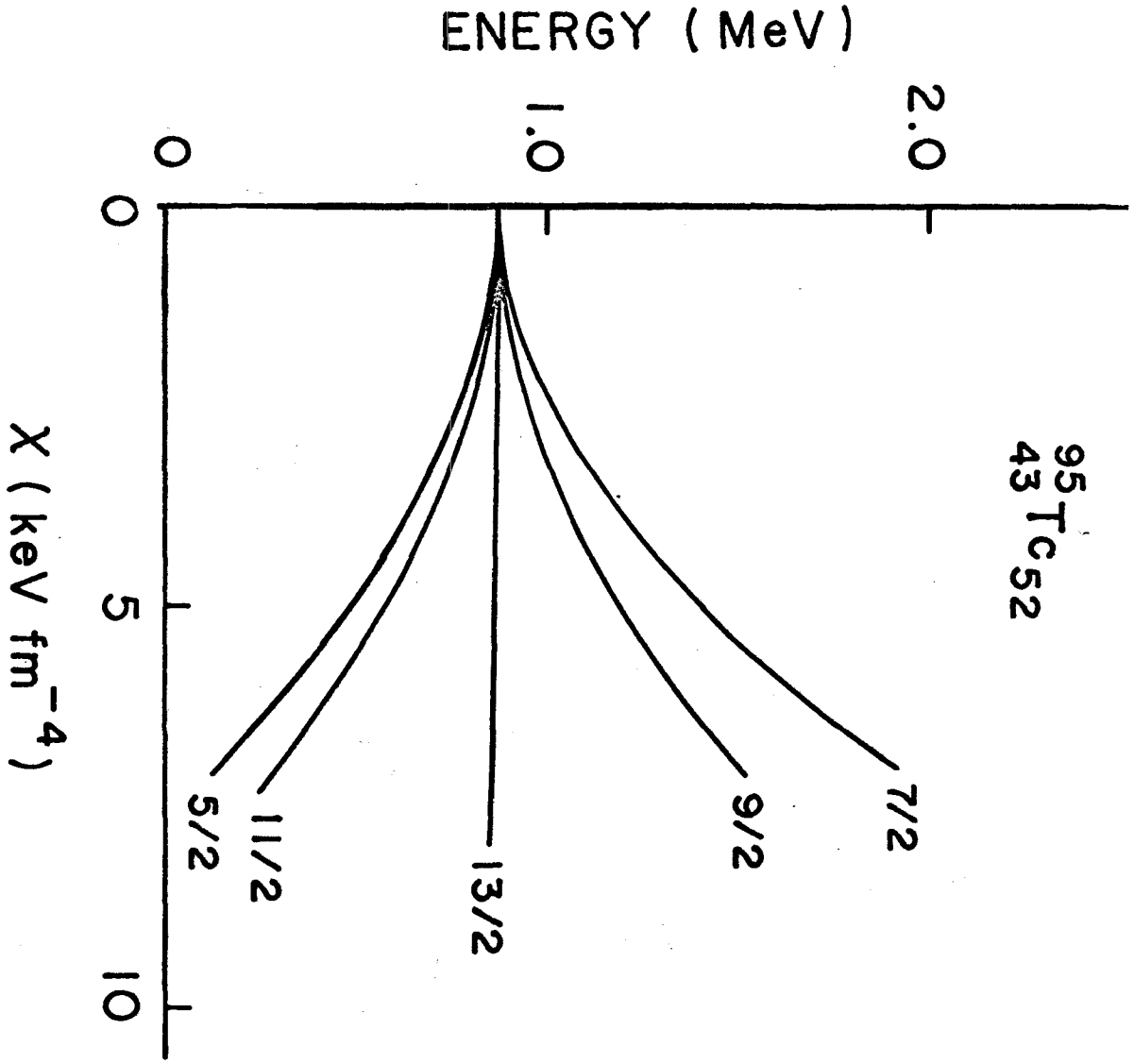

Fig. 21

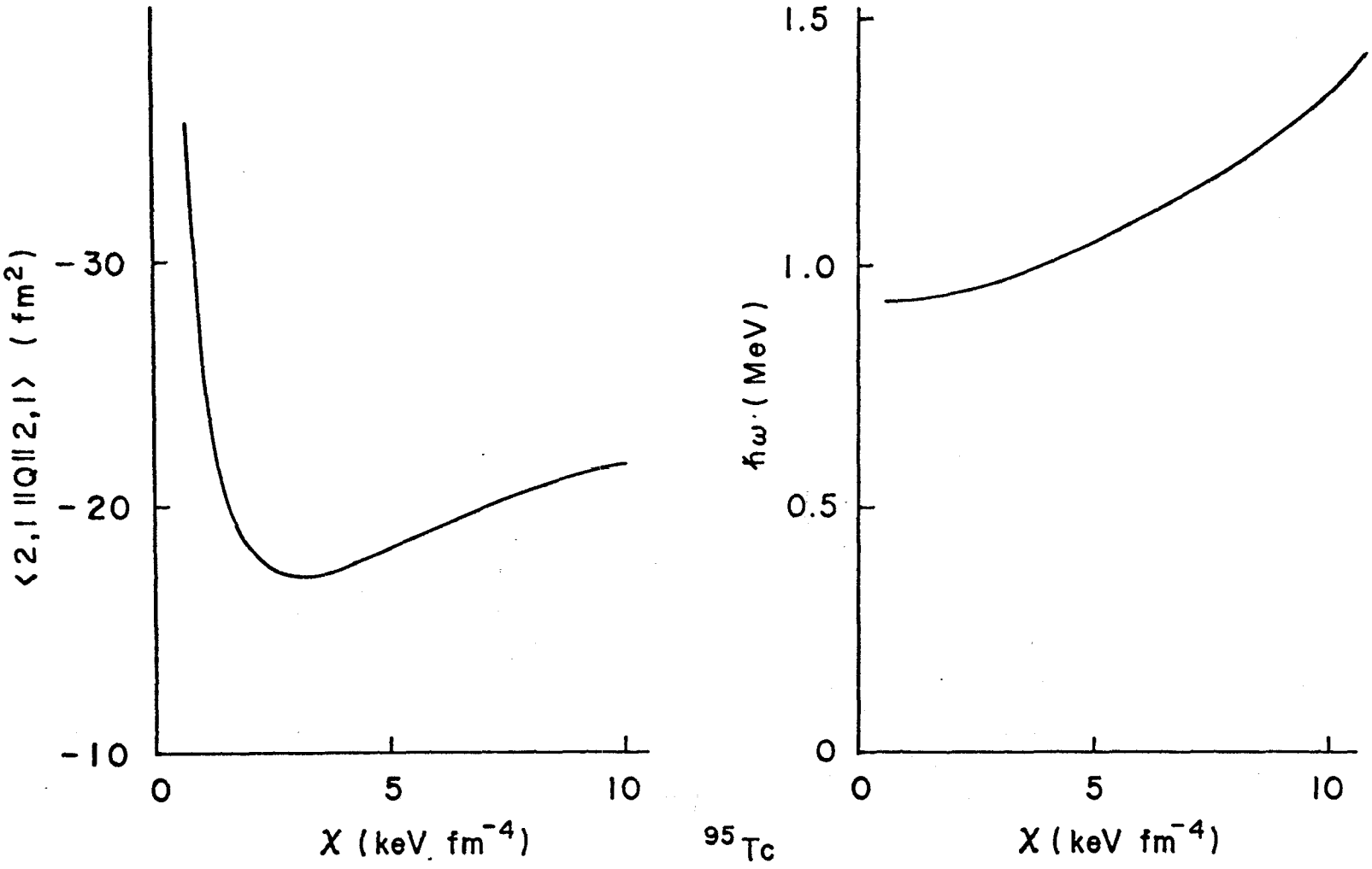
⟨2,1 ||Q|| 2,1⟩ (fm²)
-30
-20
-10
0
5
10
χ (keV fm⁻⁴)
ħω (MeV)
1.5
1.0
0.5
0
0
5
10
χ (keV fm⁻⁴)
95Tc

Fig. 22

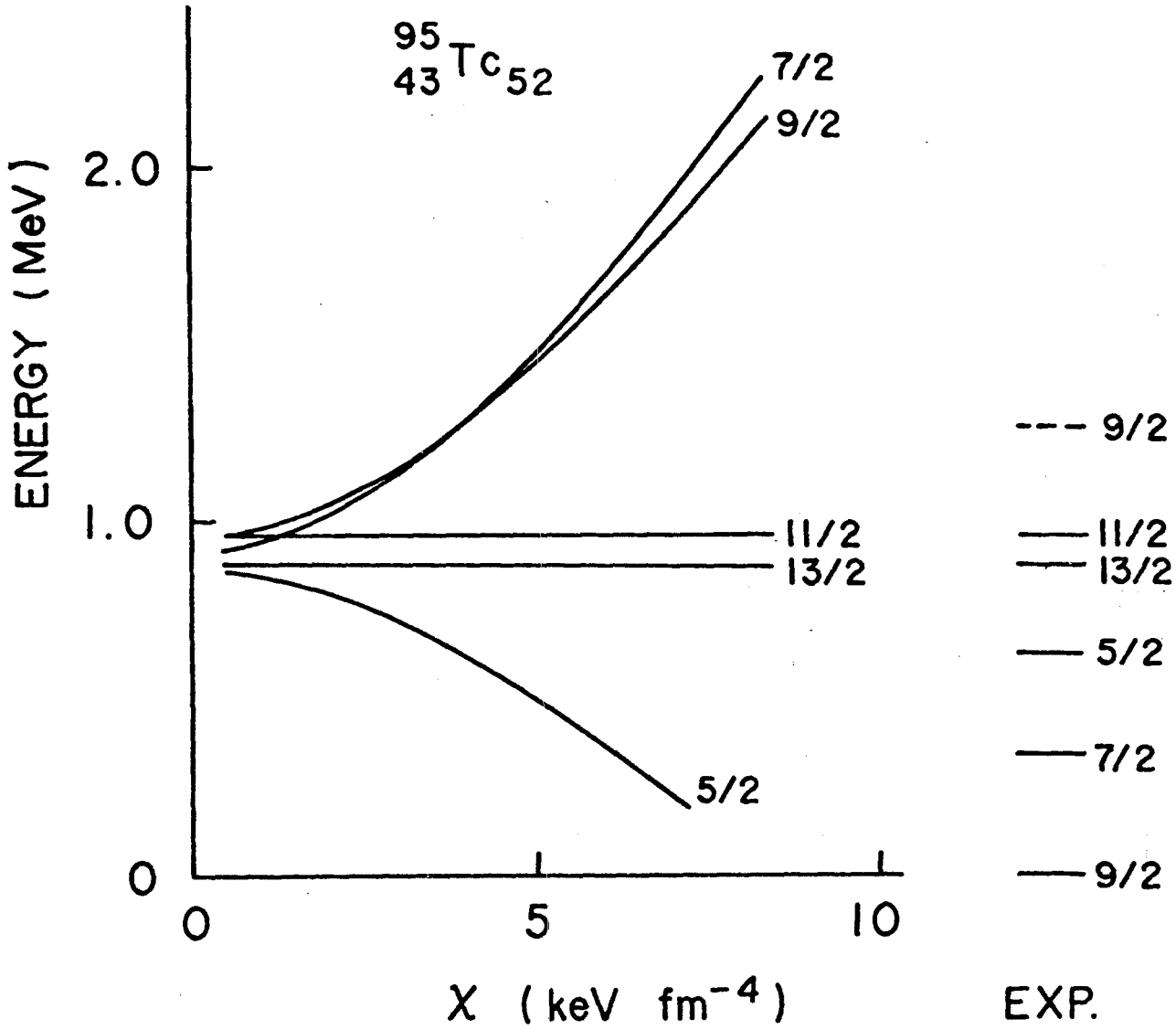
95 43 Tc 52
7/2
9/2
ENERGY (MeV)
2.0
1.0
0
11/2
13/2
5/2
0
5
10
X (keV fm⁻⁴)
--- 9/2
11/2
13/2
5/2
7/2
9/2
EXP.

Fig. 23

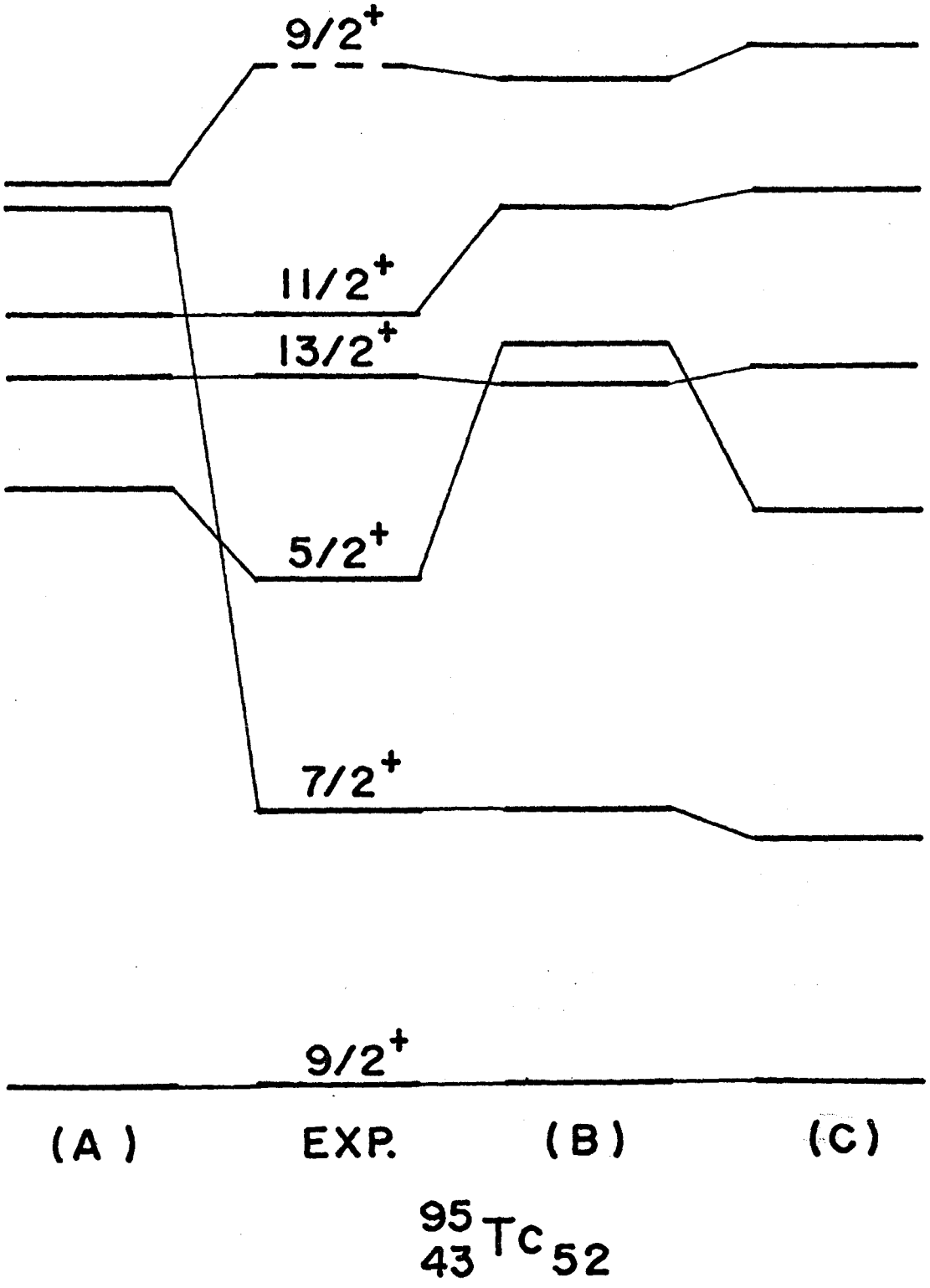

Fig. 24

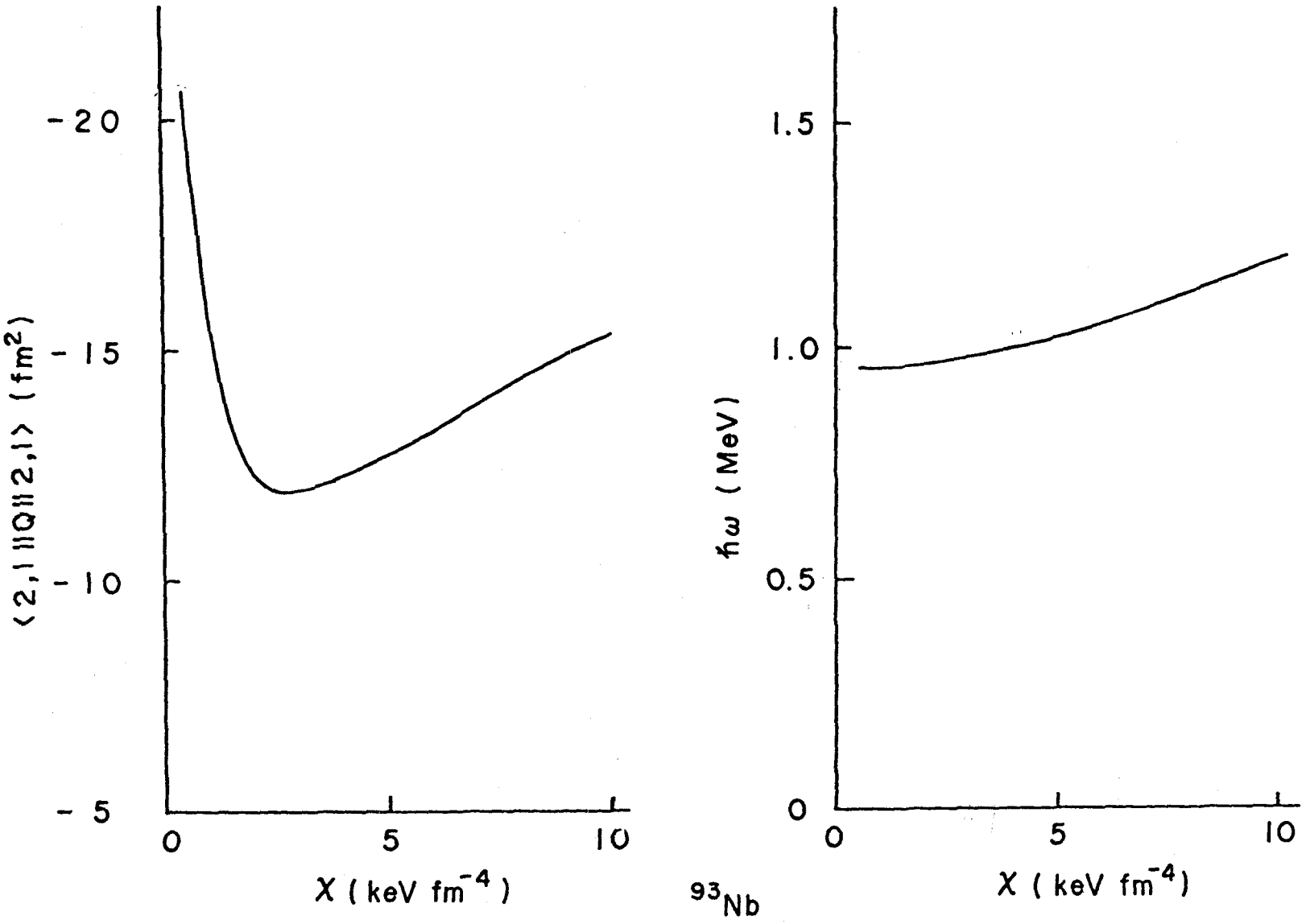

Fig. 25

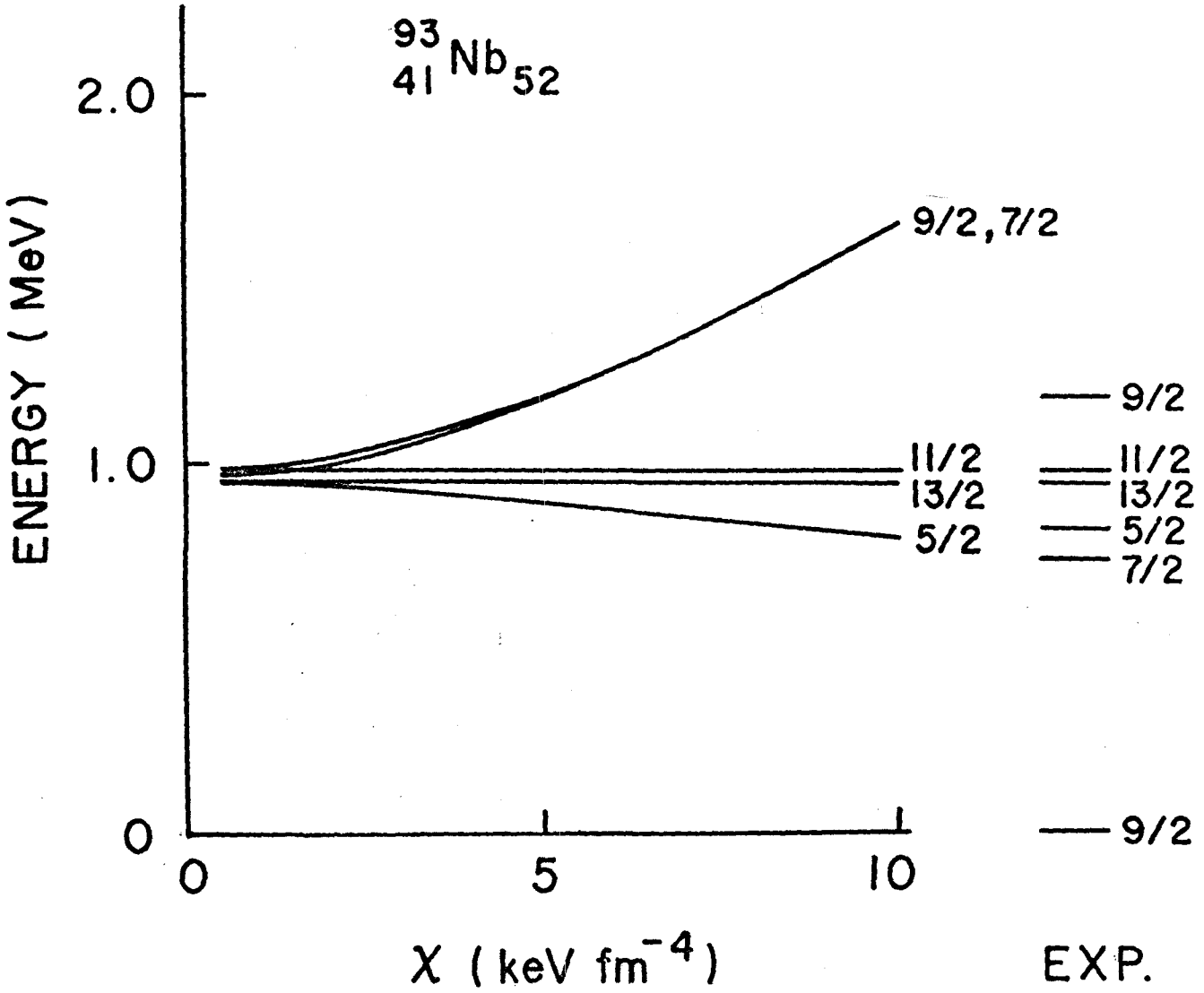
$^{93}_{41}Nb_{52}$
2.0
1.0
0
ENERGY (MeV)
9/2,7/2
11/2
13/2
5/2
9/2
11/2
13/2
5/2
7/2
9/2
0
5
10
X (keV fm^{-4})
EXP.

Fig. 26

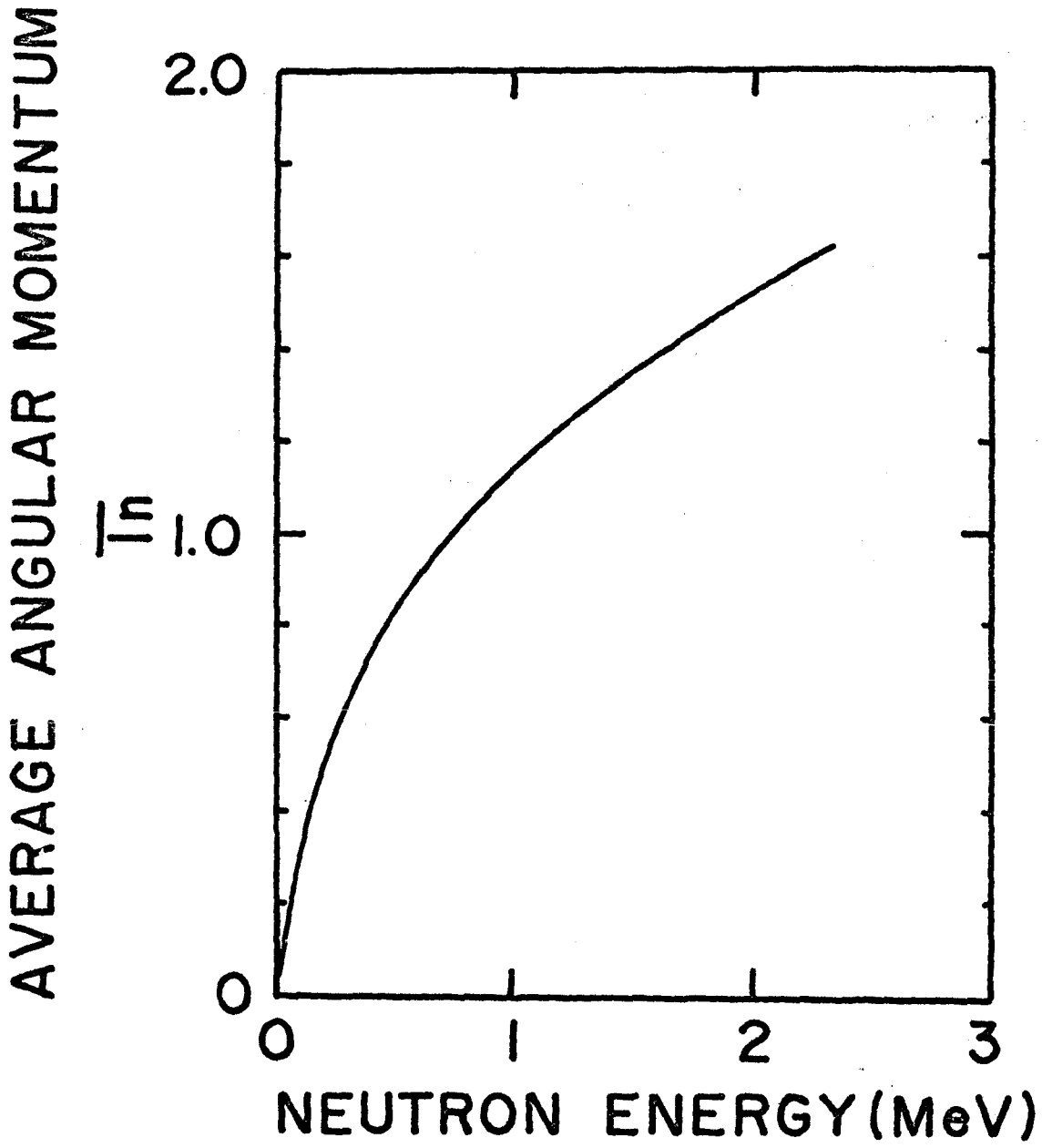
AVERAGE ANGULAR MOMENTUM
$\bar{l}_n$
2.0
1.0
0
0
1
2
3
NEUTRON ENERGY(MeV)

Fig. 27

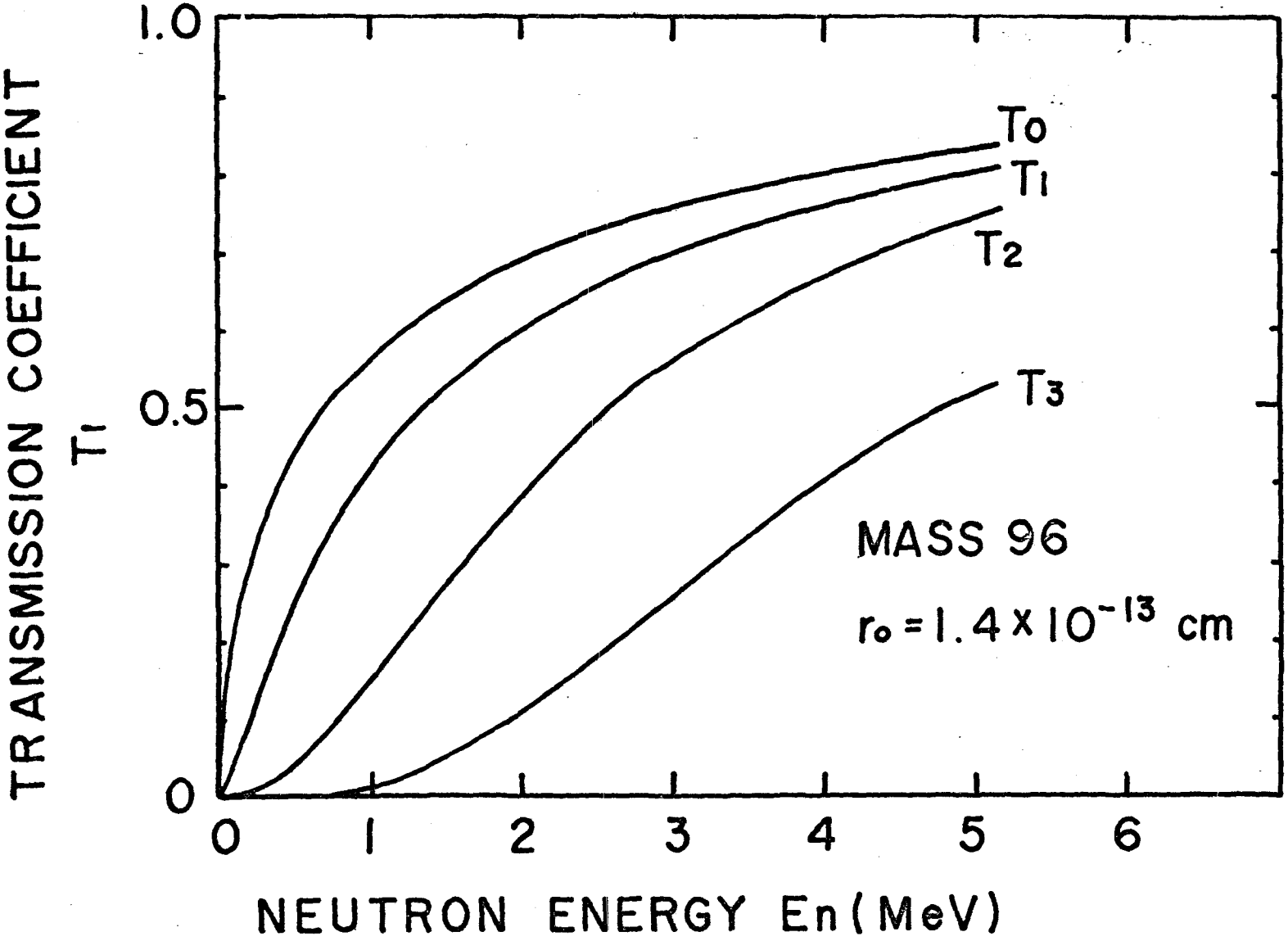
TRANSMISSION COEFFICIENT
T1
1.0
0.5
0
0
1
2
3
4
5
6
NEUTRON ENERGY En(MeV)
T0
T1
T2
T3
MASS 96
r0 = 1.4 x 10-13 cm

Fig. 28